# Impact of Biomass Sources on Acoustic-Based Chemical Functionalization of Biochars for Improved CO2 Adsorption

Riya Chatterjee<sup>a</sup>, Baharak Sajjadi<sup>a\*</sup>, Wei-Yin Chen<sup>a</sup>, Daniell L. Mattern<sup>b</sup>, Nathan Hammer<sup>b</sup>,

Vijayasankar Raman<sup>c</sup>, Austin Dorris<sup>b</sup>

<sup>a</sup> Department of Chemical Engineering, School of Engineering, University of Mississippi, 134

Anderson Hall, MS 38677-1848, U.S.A

<sup>b</sup> Department of Chemistry and Biochemistry, University of Mississippi, Coulter Hall, MS 38677

<sup>c</sup> National Centre for Natural Products, University of Mississippi, University, MS 38677, U.S.A

\*E-mail: bsajjadi@olemiss.edu, Tel No: 662-915-1640, Fax No: 662-915-7023

#### **Abstract**

The present study investigates the impact of biomass origin on the properties of biochar and its interaction with different treatment conditions, CO2 adsorption, and regeneration ability. The biochars were synthesized from eight biomasses-herbaceous (miscanthus and switchgrass), agroindustrial (corn stover and sugarcane bagasse), and crop residues (sorghum, wheat straw, rice straw, and rice husk)-and were subjected to three different treatment conditions: (I) acoustic treatment using low frequency ultrasound, (II) amination using the penta-amine, and (III) integrated sono-chemical activation. Adsorption studies revealed that sono-amination increased adsorption capacities up to 2–2.5 times that of physical or chemical activation techniques alone, with the maximum improvements for herbaceous and agro-industrial residues over crop residues due to their large specific surface areas and high carbon and low ash contents. Accordingly, miscanthus with increased nitrogen content after sono-amination (7.5 times that of raw miscanthus

biochar) showed the highest adsorption capacity compared to any other biochars. The regeneration

studies that were conducted on all of the eight ultrasono-aminated samples showed 68% (crop

residues) to 76% (herbaceous and agro-industrials) retainment of the initial adsorption capacities

after 15 cycles.

**Keywords:** Different Biochars, Ultrasound, CO<sub>2</sub> Capture, Tetraethylenepentamine (TEPA),

Amine functionalization, Adsorption

1 Introduction

Industrialization and fossil fuel combustion have increased the atmospheric CO<sub>2</sub> concentrations

from pre-industrial levels of approximately 280 ppmv to the current level of approximately 390

ppmv [1]. The atmospheric CO<sub>2</sub> concentration is predicted to increase to 1000 ppmv and 2000

ppmv by the years 2100 and 2300, respectively, if the present energy utilization structure persists

[2]. Such increases in CO<sub>2</sub> would lead to a reduction in pH and cause substantial chemical changes

in seawater carbonate systems, including increases in HCO<sub>3</sub><sup>-</sup> and decreases in H<sup>+</sup> and CO3<sup>2</sup>-.

Additionally, the increased level of CO<sub>2</sub> also resulted to increase global temperature that causes

environmental degradation and climate change. So, it is of utmost important to reduce this green-

house gas concentration to its earliest. Therefore, several remediation techniques [3] have been

adopted including

I. CO<sub>2</sub> capture from power plants and industries: This is primarily post combustion CO<sub>2</sub> capture

and utilizes different amine-based solvents.

II. CO<sub>2</sub> capture from air. This can be achieved with organics and metal carbonates and with the

use of carbonaceous sorbents.

2

Among the described techniques CO<sub>2</sub> capture using solid carbonaceous adsorbents such as biochar (a form of char produced during biomass pyrolysis under anaerobic conditions) is gaining significant attention. Based on the origin or lignocellulosic constituents the biomass can be classified as herbaceous, agro-industrial and crop based materials [4]. The further explanation on the classification has been described in the following section with its graphical representation and lignocellulosic compositional analysis in Figure 1 and Table 1 respectively.

# Figure 1, Table 1

- Agricultural Herbaceous Residue: Miscanthus (MS) and switchgrass (SG) are high yielding, low cost materials that fall in this category. These biomasses are a rich source of cellulose (40-60%) that results in their natural enrichment in carbon content (>70%) [5]. Literature study revealed that miscanthus has low macronutrient concentrations (such as N, P and K) compared to switchgrass [6]. This leads to reduced values of %N and %ash content of miscanthus biochars compared to switchgrass [6]. In addition, both these biochars possess low ash content (2-4.6%), high surface area, microporosity and micropore volume which make them highly suitable for adsorption of CO<sub>2</sub> [7-9].
- Agro-Industrial Residues: Both sugarcane bagasse and corn stover are agro-industrial residues and are inexpensive and readily available sources of lignocellulosic biomass. The biochars from SB and CS exhibit high microporosity and high chemical stability [10, 11]. As per literature study, it is evident that SB has higher %ash content and subsequently lower %carbon content than CS [12]. The macronutrient content (%N) for CS is higher than for SB [13, 14].
- Crop Residues: These are the remaining materials after crop is harvested and processed into usable resources and include sorghum (SR), wheat straw (WS), rice straw (RS) and

rice husk (RH). Biochars derived from these residues have low carbon and high ash content (13-19%), indicating the presence of minerals such as alkali metals (Ca, Mg, K) [15] specifically for biochars derived from rice husk and rice straw show high amounts of silica [16]. As a result of that, these biochars exhibit high pH values [17-19].

As discussed above the characteristics of biochars change widely according to feedstock type that has been further emphasized in Table 2 that describes different physicochemical properties of biochars prepared from different origins.

#### Table 2

As found from the literature, there are number of ways to activate biochar for the improvement of physical and chemical properties and CO<sub>2</sub> adsorption behavior such as by employing traditional physical activation technique [20]. Physical activation include partial oxidation in the presence of gaseous environments (air, CO<sub>2</sub>, or steam) under very high temperature (>750 °C) making the process highly energy intensive [21]. In comparison to this, acoustic activation can be conducted at near room temperature within a very short duration of time, making the process efficient in terms of energy and time [22]. During acoustic irradiation the formation and collapse of vapor filled microbubbles during the alternate compression and rarefication cycles of ultrasound leads to the exfoliation of the layered structure of graphitic clusters [23]. This phenomenon was first observed by Stankovich et al. where they found that a mild ultrasonic treatment (fc=78.6 kHz, 150 W) of graphite oxide in water for 1 h exfoliates its layers and forms stable aqueous dispersions [24]. Based on this observation, the previous studies conducted by our group on sonolysis of biochars revealed that ultrasound promoted exfoliation of graphitic layers of biochars along with mineral leaching and carbon and hydrogen fixation (from CO<sub>2</sub> and water, respectively), resulting in significant increments in porosity, surface area, and heating value of the biochar [25, 26]. Notably,

the effectiveness of physical activation to improve the physical properties is found to be prominent for the biochar having high lignocellulosic contents. For instance, herbaceous and agro-industrial biochars have higher cellulose and hemicellulose contents than lignin so possess high carbon content and improved microporosity (both surface area and pore volume). But crop based biochars have increased lignin contents than cellulose-hemicellulose thus exhibit low surface properties and carbon contents. Thus, origin of feedstock plays a pivotal role on properties and subsequent activation technique. While aiming to maximize CO<sub>2</sub> capture capacity, the presence of nitrogenous compound (reflected by %N content) such as amine group plays an important role as a result of the acid-base interaction between CO<sub>2</sub> and amine which subsequently boosts the adsorption efficiency [27-29]. As found from Table 2, the nitrogen content also varies according to biomass feedstock origin and substrate type [30].

Hence, the present study applied acoustic based amination technique to improve physicochemical properties and adsorption capacities of biochars. In this regard at first, a low temperature (near ambient temperature) acoustic-amination process was developed followed by the optimization of process conditions such as ultrasound duration, activating agents ratio, effect of different amines (MEA, DEA, TEPA, PEI and PZ) etc. [31, 32]. The results obtained from these studies showed that ultrasono-MEA and TEPA functionalized pine wood derived biochars intensified its CO<sub>2</sub> adsorption capacities 5-7 times than that of raw char.

Next, it was aimed to study the importance of synergistic and antagonistic interaction of the developed method with biochar structure with particular focus on biomass origin since structural and chemical properties of biochars vary depending on the lingnin, hemicellulose and cellulose contents which are governed by the feedstock sources. Thus, the main objectives of this study are I. Determination of the importance of biochars' origin on CO<sub>2</sub> removal and II. Investigation of the

response of each biochar to three different physicochemical activation processes, namely physical (ultrasonic irradiation), chemical (amine functionalization) and combined physico-chemical (ultrasono-amine) activation.

#### 2 Materials and Methods

#### 2.1 Materials

Eight different biomass feedstock were obtained from the Idaho National Laboratory namely miscanthus, switchgrass, corn stover, sugarcane bagasse, sorghum, wheat straw, rice straw and rice husk,. The chemicals utilized in functionalization were methanol, N-(3-dimethylaminopropyl-N'-ethylcarbodiimide hydrochloride (EDC, 98% purity), hydroxybenzotriazole (HOBt, 97% purity) and tetraethylenepentamime (TEPA). All chemicals were obtained from Sigma-Aldrich. Hydrochloric acid-37% (Sigma-Aldrich), acetone (Sigma-Aldrich) and sodium hydroxide (Fisher Scientific) were used during the filtrations of the functionalized biochars. Deionized water used in the experimentation was obtained from Milli-Q ultrapure water tap (Millipore Sigma). All chemicals used were of analytical grade.

# 2.2 Experimental Method

## 2.2.1 Pyrolysis of biochar

At first, the as-received biomasses were ground using an IKA MF10 basic continuous feed grinder and sieved using a Gilson SS 15D 8-in sieve shaker to particles of size range 75–250 μm. The sieved biomasses were dried under vacuum overnight at 60 °C prior to pyrolysis. Nickel-chromium-iron alloy Inconel crucibles were used for the pyrolysis. The crucibles were filled with biomasses, covered with lids and placed inside a muffle furnace (in triplicate) for pyrolysis. The covered crucibles were heated up to 600 °C with a 20 °C/min heating ramp under nitrogen flow.

The temperature was held at 600 °C for 2 hrs. and then allowed to cool to room temperature under nitrogen flow.

# 2.2.2 Physical Activation of Biochar under Acoustic Treatment

For physical activation, 3 g of biochar was subjected to low frequency ultrasonic irradiation (QSonica sonicator model no. Q700) in 250 ml of water for 30 s. Our previous study demonstrated that 30 s of acoustic irradiation was enough to induce surface area enhancement [31]. In contrast, prolonged sonication diminished the effect of ultrasound on surface area enhancement, most likely through disarranging the orientation of the layered structures and blocking pores [31]. This observation is in accordance with the literature [32, 33]. The ultrasonicated biochar-water mixtures were subjected to the following chemical activation steps without further treatment.

#### 2.2.3 Chemical Functionalization of Biochar with TEPA

Raw or physically activated biochar-water mixtures were treated with the coupling agents EDC-HOBt (3.375 g of each coupling agent for 3 g of biochar) [31]. EDC is highly soluble in water compared to the other coupling agents (such as dicyclohexylcarbodimide – DCC) which makes its separation very easy. The additive HOBt was used to prevent an undesired side reaction that could reduce the yield of the product where the ratio of EDC: HOBt kept at 1:1 ratio. The EDC-HOBt-biochar mixture was kept under stirring for 24 hours at 35°C, then filtered and dried under vacuum at 60°C overnight. Next, the dried samples were suspended in methanol, and TEPA (2.5 times weight to the weight of biochar) was added to the suspension. The resultant mixture was stirred for 24 hours with gentle heating as before. Finally, the resultant mixture was filtered and washed in succession with 200 mL of 1N NaOH (3 times), 200 mL of 1N HCl (3 times) and 200 mL of acetone (1 time) and dried as before.

#### 2.3 Characterizations of the Adsorbent

The following characterization techniques were applied to both raw and functionalized chars. First, the surface morphology was determined using scanning electron microscopy (JSM-7200 FLV by JEOL). Textural properties such as specific surface area and pore volume were examined using BET sorptometry (Micromeritics TriStar II 3020, Malaysia). The adsorption isotherm study was conducted under liquid nitrogen environment at 77 K and the technique measures volume adsorbed by the sample as the relative pressure is gradually increased from 0 to 1. Then, the mesopore area and pore volume were calculated by the BET (Brunauer, Emmett and Teller) equation:

$$\frac{1}{v\left[\left(\frac{p}{p_0}\right)-1\right]} = \frac{c-1}{v_m c} \left(\frac{p}{p_0}\right) + \frac{1}{v_m c} \tag{1}$$

Where p,  $p_0$ , v,  $v_m$ , c respectively represent equilibrium pressure of adsorbate at the temperature of adsorption, saturation pressure of adsorbate at the temperature of adsorption, adsorbed gas quantity, monolayer adsorbed gas quantity and BET constant.

The t-plot based on the de-Boer equation was also used to calculate micropore surface area and pore volume.

$$p = K_2 \frac{\frac{v}{v_m}}{1 - \frac{v}{v_m}} \exp\left[\frac{\frac{v}{v_m}}{1 - \frac{v}{v_m}} - K_1 \frac{v}{v_m}\right]$$
 (2)

Where p, v,  $v_{m,i}$   $K_2$ ,  $K_1$  respectively represent equilibrium pressure of adsorbate at the temperature of adsorption, adsorbed gas quantity, monolayer adsorbed gas quantity, parameter related to the gas-solid interaction which are function of temperature and the properties of the adsorbate.

Mesopore area is calculated by subtracting t-plot area from the BET surface area. In the similar way t-plot micropore volume is subtracted from total pore volume to get meso pore volume.

Elemental compositions were determined through C, H, N, S, O, ash analysis (Huffman Hazen Laboratory, Colorado, USA). The changes of the chemical functional groups and the chemical

structure before and after activation were assessed using Fourier Transform Infrared (FTIR, Cary 660 FTIR Agilent) and Raman (LabRam HR Evolution) spectroscopies.

### 2.4 CO<sub>2</sub> Adsorption Studies

The CO<sub>2</sub> adsorption tests were conducted in a tubular reactor made of alumina oxide, which was placed inside a temperature-controlled furnace. The details experimental set up has been represented in Figure 2 with the descriptions of each part and their functions. For each run, 2 g of biochar sample was placed inside the reactor, degassed using helium (99.99%) at a flow rate of 500 cm<sup>3</sup> min<sup>-1</sup> at 378 K for 1 hour, and then cooled to 333 K. This temperature was kept constant throughout the course of the reaction. In the next step, the helium gas was switched to a CO<sub>2</sub>-containing simulated flue gas of 10 vol.% CO<sub>2</sub> balanced with He at the same flow rate, and was allowed to interact with the adsorbent. The CO<sub>2</sub> concentrations before and after adsorption were measured by a CO<sub>2</sub> analyzer (ZRH Infrared Gas Analyzer, California Analytical Instruments) connected to the adsorption column. The detection limit for the CO<sub>2</sub> concentration is up to 20 vol.% with repeatability of 0.5% of full scale.

The adsorption capacity of CO<sub>2</sub> after a certain time was then calculated using the following equation:

$$q_a = \frac{1}{M} \times \left[ \int_0^t Q \times (C_0 - C) dt \right] \times \frac{1}{V_m}$$
(3)

where,  $q_a$  is the adsorption capacity for  $CO_2$ , mmol  $g^{-1}$ ; M is the mass of adsorbent, g; Q is the gas flow rate, cm<sup>3</sup> min<sup>-1</sup>;  $C_0$  and C are influent and effluent  $CO_2$  concentrations, vol.%; t denotes the time, min; and  $V_m$  is 22.4 mL mmol<sup>-1</sup>.

# 2.5 Regeneration Study

Thermal swing adsorption-desorption experiments have been conducted to determine the stability or the regeneration capacity of the adsorbents. To study this, ultrasono-amine functionalized adsorbents (prepared from all the eight different biomasses) have been used. Regeneration experiments were conducted by heating the adsorbent at the elevated temperature of 453 K under helium gas flow for 60 minutes followed by adsorption experiment at 333K. For each adsorbent, 15 adsorption-regeneration cycles have been carried out.

#### 3 Results and Discussions

## 3.1 Surface Area Analysis

Effect of Feedstock Origin: Surface area is one of those factors that significantly affects the adsorption capacity of solid sorbents. Table 3 represents the surface area and pore volume of raw, ultrasonically activated, aminated, and sono-chemically activated chars which are reported with the symbols R, US, Am, and US-Am, respectively. In terms of raw biochar origins, micro and mesopore surface areas and volumes all followed this decreasing order: herbaceous biochars (MS, SG) > agro-industrial residues (CS, SB) > crop residues (SR, WS, RH, RS). This is consistent with the elemental compositions of the synthesized biochars that demonstrate a roughly increasing trend of %ash contents following the same order (Table 4). The ash generated during pyrolysis remains trapped inside the pores of the biochar, thus lowering the surface area [34]. The surface area trend can be further explained based on the inherent physical and chemical properties of different lignocellulosic biomasses. Lignocellulosic biomasses contain hemicellulose (40–50%), cellulose (20–40%) and lignin (10–40%) [35]. Decomposition of hemicellulose takes place mainly at 250–350°C, followed by cellulose at 325–400°C and lignin at 300–550°C [35]. The biochars that are primarily composed of cellulose and hemicelluloses, with lesser lignin contents, decompose

easier and possess higher surface areas [36]. As found in Table 2, herbaceous (MS, SG) and agro industrial residues (CS, SB) tend to have elevated cellulose and hemicellulose contents, indicating higher surface areas over crop residues (SR, WS, RS RH) that possess higher lignin and lower cellulose-hemicellulose contents.

Effect of ultrasound: Ultrasound activation significantly increased the surface area and pore volume of micropores in all biochars, without any exception. Ultrasound cavitation and its implications result in the exfoliation of the graphitic cluster of the biochar structure, leaching of mineral matters and opening of the pores (which otherwise remains blocked) and lead to enhancement of microporous surface area [24-26, 37, 38]. Sonication resulted in increased microporosity by up to 50-71% and the extent of increase followed this trend: crop residues: WS (71%) > RH(63%) > RS(60%) > SR(57%); agricultural residues: SB(55%) > CS(50%) and herbaceous residues: MS(53%) > SG(50%). This trend suggests that acoustic activation has a higher effect on biochar containing more mineral matter or ash (referring to Table 4). However, the overall trends for US-treated chars were the same as for raw chars; that is, the maximum and minimum surface areas were observed for miscanthus (520 m²/g) and rice straw (242 m²/g), respectively.

Unlike microporosity, mesoporous surface area was slightly reduced upon sonication due to the formation of small aggregates (that form micropores) and partial destruction of mesopores under ultrasonic irradiation [39]. As found in Table 3, MS possessed the maximum (61 m²/g) and RS the minimum (22 m²/g) mesoporous surface area. Biochar samples with highest and lowest surface areas (both microporous and mesoporous) also had the maximum and minimum pore volumes. For instance, US-MS had the highest microporous surface area (520 m²/g) and pore volume (0.17

cm<sup>3</sup>/g), whereas US-RS had the lowest surface area (242 m<sup>2</sup>/g) and pore volume (0.08 cm<sup>3</sup>/g). Similar trends were obtained for mesopore volume.

Effect of amination: Amines can be attached to the porous structure of biochar either through impregnation or through grafting. During impregnation, amine molecules are dispersed into the pores over internal and external surfaces through weak van der Waals forces [40]. While grafting involves attachment of amine to the surface functional groups through strong covalent bonds. In either of the mechanisms, the amine diffuses into either micro or mesopores without destroying the intrinsic structure of the sorbent, resulting in reduced sorbent surface area [40, 41]. Similar observations have been reported by Yue et al. and Teng et al. [42, 43] and also found in our previous studies [31, 38]. Consistent with this, the present study also revealed that micro and mesoporous surface areas and the corresponding pore volumes decreased after amine functionalization. Micro and mesoporous surface areas were reduced by 38-50% and 22-33%, respectively compared to raw chars. In accordance with the initial surface areas, MS demonstrated the highest (170 m<sup>2</sup>/g) and RS the lowest (90 m<sup>2</sup>/g) microporous surface area values. The following decreasing trend for microporous and mesoporous surface areas and pore volumes can be obtained (Table 3) - herbaceous residues: MS > SG; agricultural residues: CS > SB; and crop residues: SR > WS > RH > RS (micropores) and SR > RH > WS > RS (mesopores). Reduction in surface area corresponds to quantity of amines attached and consequently to improved adsorption capacity. Effect of sono amination (compared to raw and aminated biochar): Sono-aminated biochars showed lower surface areas than raw chars, but the values were notably higher than aminated chars (without acoustic treatment). Generally, the sono-aminated biochars had 4-38% higher surface areas than aminated BC's (without acoustic treatment). This is because of the acoustic treatment which greatly enhanced microporous surface area, before it was lowered by amination. Consistent with the previous trend, MS exhibited the maximum (207 m²/g) and RS the minimum (106 m²/g) surface area with reductions of 39% and 30% with respect to raw char, but increases of 22% and 18% compared with aminated chars. On the other hand, mesoporous surface area showed a different trend because of its reduced value after sonication, which would lead to further lowering of the surface area after amine grafting, with reductions of 28-39% with respect to raw and 2-22% with respect to aminated chars.

The surface areas for the sorbent materials can be further described using the adsorption isotherm plots as shown in Figures 3-6. The isotherm plots correlate the amount (volume) of gas adsorbed by the adsorbent with respect to the relative pressure. The higher the adsorbed volume, the better will be the surface area and pore volume. Comparing the figures, it can be observed that sonicated biochar samples exhibit the highest value for the adsorbed volume corresponding to their maximum surface area than any other biochar samples. Aminated samples have lesser adsorbed volume than both raw and sonicated samples indicating their lower surface area. The ultrasono-aminated samples have adsorbed volumes higher than aminated chars but lower than raw samples which are consistent with their corresponding surface area and pore volumes (Table 2).

In addition to that the isotherms also characterize the adsorbent materials in terms of their porosity. For instance, the shape of the above described isotherms are similar to Type I isotherm (as per IUPAC classification) which are common for microporous solids [44]. Type I isotherm is usually observed when the attractive forces between adsorbed gas and adsorbent are greater than those between the molecules of the gas [44]. Hence, the isotherms further provide a confirmation of the porous nature of the adsorbent materials [44].

Hence, surface area analysis along with the adsorption isotherms revealed that herbaceous biochars provided the maximum surface area and porosity than agro-industrial and crop based chars.

## 3.2 SEM Analysis

Surface morphology of the raw biochars (prepared from different biomass sources) and ultrasound activated biochars are presented in Figures 7-9. Herbaceous biomasses such as raw MS and SG both exhibited (Figures 7a and 7c) structural similarity, having smooth and non-porous surfaces. As observed from their surface morphology, these samples possessed a comparatively thicker tubular structure (see arrows in Figure 7a; ca. 100 µm) than agro-industrial and crop based biochars (for example, see arrows in Figure 9b, ca. 10 µm). When exposed under ultrasound irradiation, the induced microjets penetrate the structure, resulting in significant increment of surface porosity as observed in Figures 7b and 7d. Alteration and disarrangement of the layer was less pronounced for these chars; thus a uniform pore formation and opening of porous structure was observed for MS and SG. This is consistent with the surface area analysis (Table 3) that demonstrated MS and SG possessed the highest microporous surface area and pore volume upon ultrasonication. These properties favor CO<sub>2</sub> adsorption capacity; thus MS and SG possessed maximum adsorption capacities compared to other biochars.

Figures 8a and 8c describe SEM images of raw CS and SB biochars. The surface layers of these biochars are thinner than those of MS and SG. As a result of this the ultrasound waves disarrange the biochar structure significantly than the herbaceous residues, as seen in Figures 8b and 8d. As found from the Figures 8b and 8d, CS and SB showed low porosity along with the severe structural deformation under sonication. Notably, for SB, the pores that formed got disrupted (Figure 8d), resulting in low microporous surface areas and pore volumes (Table 3) and significant ash reduction (Table 4). As a result, the biochars of this category showed intermediate CO<sub>2</sub> adsorption capacities.

Figures 9a, 9c, 9e, and 9g portray surface morphologies for raw SR, WS, RH and RS samples. As per the figures, SR, WS and RS showed similarity in structure. Notably, RH had swollen surfaces attributed to its high silica content. Similar to agro-industrial residues, these chars also possessed relatively weak structures. Thus the raw chars underwent significant disarrangement when exposed to acoustic field (Figures 9b, 9d, 9f, 9h), resulting in small fragments and destruction of porosity (Figure 9d) with significant reduction in ash contents. As a result, the obtained surface area was very low, consistent with their limited adsorption capacity.

Thus, the SEM images revealed that herbaceous biochars have more rigid structure compared to agro-industrial and crop based chars that promote uniform pore generation under acoustic field and enhanced CO<sub>2</sub> adsorption capacities.

# Figures 7-9

## 3.3 Elemental Analysis

Effect of Feedstock Origin: Elemental compositions of raw biochars and biochars activated under different conditions (ultrasonically, chemically, or ultrasono-chemically), as well as their organic-only compositions omitting ash, are presented in Tables 4 and 5, respectively. The results (Table 4) show that raw herbaceous biochars (MS and SG) had a higher %C content (77-82%) and lower %ash content (4.35-12.78%) compared to the most of the other chars (except CS for %ash). The %C followed a similar trend for organic-only composition (Table 5). Intense carbon concentration of MS and SG can be ascribed to their rich cellulose content (Table 2). For both chars, %O and %H content was found to be between 9.68-11.2% and 2.04-2.32%, respectively. The %N content of MS-biochar was about half that of SG-biochar because of the lower macronutrient concentrations (such as N, Ca, K) of MS in comparison to SG [6]. This higher carbon and lower nitrogen content of MS results in its high C/N value (343) relative to SG (158) as found from Table

5. The low macronutrient concentration of MS further leads to its low %ash content and pH value (8.77) compared to other chars (> 9.48). These results are consistent and comparable with the literature [7, 45].

Agro-industrial residues (raw CS and SB) had %C contents between 68.10-74.47% (Table 4). However, bagasse showed higher %ash content (19.78%) than corn stover (12.00%) despite the higher pH for CS (11.56) compared to SB (9.48). These observations are in accordance with the literature as discussed in Table 1. Mineral content of CS primarily consists of Ca, Mg and K whereas SB mostly consists of Zn, Fe and K [14, 45]. The presence of minerals such as Ca and Mg can significantly increase the pH of biochars, which has been observed for CS despite its low ash content [46]. Both of these biochars had considerably high carbon content (though lower than that in herbaceous biochars) with comparable oxygen and hydrogen content. The %N content of CS was higher than SB as a result of the higher macro element content (%N) of CS biomass [13, 14]. This resulted in a higher C/N ratio for SB (162) than for CS (107).

Crop residues tend to have comparatively lower %C and higher %ash contents than the two preceding biochar categories. Biomass combustion research has shown that feedstocks containing more silica have relatively high slagging tendencies and relatively high ash content [47]. Silica content (RH > RS > WS) and alkaline elements (Na, K, Ca, Mg) contribute to high ash and pH values [48, 49]. Thus, WS, RH and RS exhibited higher ash contents than SB and accordingly lower carbon contents, with pH in the range of 9.9-11.54. In crop residue-based biochars, RH (with the highest silica content) represented the lowest pH value, though it contained the maximum ash. In contrast, SR, with the lowest ash percentage, had the highest pH (11.72), since it is a rich source of minerals like Ca, Mg, K [46, 50]. A similar trend was also observed for CS, which showed low ash (12%) but high pH (11.56) [17]. On the other hand, elemental nitrogen contents of this group

showed more elevated values than herbaceous and agricultural based biochars, except for RH. As a result, RH exhibited the highest C/N ratio in this group, followed by SR, WS and RS.

Effect of ultrasound: As already stated, the cavitation phenomenon exfoliates biochar structure and leaches out mineral matters, thus lowering ash content and increasing carbon content [51]. As might be expected, biochars with comparatively higher ash contents, such as WS, RH and RS (crop residues), showed significantly greater ash loss (losing from 14 to 19 %ash) under ultrasound irradiation in comparison to herbaceous (MS, SG) and agro-industrial (CS, SB) biochars, along with SR (the crop residue having the lowest ash content), that lost between 0.4 and 3.3 %ash. The substantial ash removal caused significant increases of %C and reductions of %O content in most biochars. Oxygen reduction could be attributed to removal of inorganic oxygen of mineral compounds. Similar results were also found in our previous studies [25, 26, 38]. However, CS and RS showed %O increments (Table 5). The reason for oxygen increase may be related to increased oxygen functionality as a result of exfoliation of biochar structure [26]. Increases in %O content of CS and RS subsequently reduced its percentage of C (Table 5). In addition, the physically activated biochars showed slight increments of %N content, compared to raw biochars, in herbaceous residues MS and SG, and agro-industrial biochar CS (Table 5). On the other hand, reduction in nitrogen content was observed in crop residue biochars (Table 5). Because of their slight enhancements in %N content, MS, SG, and CS biochar samples showed reduced C/N ratios, while the opposite trend was observed in SB, SR, WS, RH and RS chars.

Effect of amination: TEPA-aminated biochar samples without sonication showed mineral (ash) leaching and subsequent variations in %C content. Removal of some ash from the biochar structure could be attributed to the washing away of mineral contents of the biochars during aqueous modification procedures [52]. As expected, the %N content of TEPA-functionalized samples

increased in the range of 1.4 - 4 times compared to raw chars (Table 5). Therefore, the C/N ratio of TEPA-treated samples showed a notable reduction compared to raw char as a result of incorporation of TEPA (C/N = 1.37). Following amination, the %N was lowest for the herbaceous residues (1.2-1.4%), higher for the agro-industrial biochars (1.4-1.6%), and, except for RH (1.4%), highest for the crop residues biochars (2.1-3.5%) with the order of (Table 5): RS>WS>SR>SB>RH=CS=SG>MS.

Effect of sono amination (compared to raw biochar): Sono-amination resulted in increased ash contents for three of the samples (MS, SG, WS) with respect to raw chars, exceptionally so for MS and WS. The increased ash contents for these chars are associated with a significant reduction of %C. For the other sono-chemically treated biochars, a reduction of ash content and an accompanying increase in %C were observed, exceptionally so for SB, SR, and RH. As a result of amalgamated sono-chemical treatments, most activated samples showed somewhat increased values of %H compared to raw chars, excluding RH (Table 5). TEPA functionalization resulted in increased nitrogen content for all the biochar samples. Sono-aminated RH, WS and MS showed the highest gains in %N content and SR showed no change with the following overall order and %increment of nitrogen content for the samples, based on Table 5: RH (1.7) > WS (1.6) > MS (1.5) > RS (1.2) > SG (0.9) > CS (0.6) = SB (0.6) > SR (0). In addition, for CS, SB, RH and RS, amine grafting slightly lowered %O content (compared to raw BCs) because TEPA has no oxygen (Table 4). Also, for SR and RH the significant reduction in %ash content resulted in overall increases of %C, %H, %O and %N (Table 4).

Effect of sono amination (compared to aminated biochar): The %C content of sono-aminated chars showed some fluctuations compared to aminated ones; however, organic analysis (omitting ash content, Table 5) suggested that sono-amination did not significantly change the %C content of

biochar compared to aminated chars (without US). Similarly, oxygen and hydrogen contents of sono-aminated samples did not change significantly compared to the aminated ones. The slight increase or reduction of O content is mainly observed due to ash changes in the carbonaceous structure of the biochars. %N contents of physico-chemical activated chars showed increases compared to aminated biochars in most cases because sono activation further aided in attaching more amine moieties by increasing surface area. The only significant reductions of amine grafting compared with amination alone were observed in sono-aminated SB and SR (Table 5).

Comparing the results of elemental analysis from both Tables 4 and 5, it can be inferred that the combined acoustic-amine activation approach was effective in terms of increasing the nitrogen content of biochars owing to their modified textural properties under ultrasound irradiation, which subsequently improved the functionalization efficiency.

#### Tables 4-5

## 3.4 FTIR Analysis

Effect of Feedstock Origin: FTIR spectroscopy is an analytical technique that can identify the changes in surface functional groups of biochar. FTIR spectra of raw, ultrasonically activated, amine activated and sono-chemically activated samples are presented in Figures 10-13. To have a correct comparison of the intensity of the peaks, the baselines of the graphs were revised in Origin lab (Version 2019b). The original IR plots are shown in Supplementary Data (Figures 22-25). Thermal destruction of cellulose and lignin during pyrolysis results in the exposure of aliphatic – CH<sub>2</sub>—, hydroxyl –OH, and C=O functional groups in biochars [53]. As a result of that, all raw biochars showed O-H stretching vibrations of hydrogen bonded hydroxyl groups at 3300-3600 cm<sup>-1</sup>. The source of the unusual asymmetric peak around 2600 cm<sup>-1</sup> is unclear. A peak at 2300 cm<sup>-1</sup> is attributed to CO<sub>2</sub> absorption [54]. A peak around 2100 cm<sup>-1</sup> is likely an overtone of the C-O peak

near 1050 cm<sup>-1</sup>. A peak at 1600 cm<sup>-1</sup> is ascribed to carboxylate (COO-), 1° amine N-H bending, or aromatic C=C stretch [55], and alkyl CH bending can appear around 1400 cm<sup>-1</sup> [56]. The peak in the region of 1026 cm<sup>-1</sup> is typical of C-O stretching vibrations (which suggests the pyranose C-O structures from cellulose were preserved to some extent after pyrolysis) and/or the CNH<sub>2</sub> stretch of an aliphatic primary amine [57]. Aromatic C-H deformation in the region 465-832 cm<sup>-1</sup> indicates the presence of aromatic hydrogen and a greater degree of aromaticity of the sample [58-62].

Raw biochar samples showed strong C-O stretching vibrations in the region 1000-1200 cm<sup>-1</sup> with the following order: RS>RH>SB>WS>MS>SR>CS>SG. With the exception of RS, RH, and SG, this roughly follows the trend of ligninocellulosic compositions given in Table 2. The strong peak for RH in the region 1000-1100 cm<sup>-1</sup> is partly due to the presence of a high amount of silica that overlaps the C-O peak [57, 63]. The same region for RS may be partly attributed to 1° amine C-N stretch, which correlates to its elemental composition that shows very high %N (highest among all raw chars) [57]. In addition, the COO<sup>-</sup> (carboxylate) peak at 1600 cm<sup>-1</sup> is strong for the MS sample, which is consistent with the high O content of this biochar (Table 4).

Effect of ultrasound: The spectra of physically activated biochar samples (Figs 11 and 23) showed lowered % transmittance compared to raw samples which can be explained because of the reduced particle size upon sonication [64]. Moreover, sonication resulted in the peaks becoming more distinct and intense. For instance, the peaks between 1500-1700 cm<sup>-1</sup> (C=O) and 3300-3600 cm<sup>-1</sup> (O-H group) became more intense, as did the CO<sub>2</sub> signal at 2300 cm<sup>-1</sup> and the peaks for C-H (at 832 cm<sup>-1</sup>) and C-H (at 1400 cm<sup>-1</sup>). As per the figure, C-H deformation at 800 cm<sup>-1</sup> is more prominent in crop based biochars than agro-industrial and herbaceous based biochars. These results are consistent with the textural property analysis (Table 3) of ultrasonically treated biochars that showed the following trend for % enhancement of microporous surface area and its

corresponding pore volume: crop residues: (WS>RH>RS>SR) > agricultural residues: (SB>CS) > herbaceous residues: (MS >SG).

Effect of amination: Effect of amination (no ultrasonication) on surface functional groups can be observed from Figures 12 and 24. The peak in region ~1600-1700 cm<sup>-1</sup> was intensified, indicating possible incorporation of NH2 groups. A similar trend was observed for IR peaks for agroindustrial based chars CS and SB. In addition, the strong peak at 1000-1100 cm<sup>-1</sup>, which is partly attributed to the attachment of aliphatic amine, is intense for all aminated biochar samples, except for aminated MS and RS that didn't show any significant change in peak intensity. On the other hand, increased nitrogen content of aminated MS, SB and RH compared to raw samples is consistent with their strong IR peaks observed at 1600 cm<sup>-1</sup> (NH<sub>2</sub>) and 1100 cm<sup>-1</sup> (C-N). Effect of sono amination (compared to raw biochar): The spectra of sono-aminated chars are depicted in Figures 13 and 25. As discussed earlier, the intensified peak around ~1100 cm<sup>-1</sup> (C-N bond) is because of attachment of aliphatic amine. This peak follows the trend of RS>WS>CS>SG>MS>SR>SB>RH, with prominent changes for SG and CS. A sharp peak around 1600 cm<sup>-1</sup> is observed due to contributions from COO<sup>-</sup> and NH<sub>2</sub> groups for MS and CS. Comparing these trends with elemental analysis it can be suggested that MS and CS showed significant improvement in nitrogen content, suggesting their enhanced sorption abilities towards CO<sub>2</sub> (Figure

Effect of sono amination (compared to aminated biochar): Mostly, the spectra of sono-aminated samples have similar trends as those observed for aminated samples. The observed differences can be attributed to the variation in intensity of the peaks as a result of the attachment of higher number of amine moieties following activation. Strong C-N stretch attributed to aliphatic amine has been observed in region 1100-1200 cm<sup>-1</sup> for most of the sono-aminated samples, except that SB and SR

12).

show weaker peaks than aminated-only chars. Peaks at 1600 cm<sup>-1</sup> may be stronger for ultrasono-aminated samples than for aminated chars. Accordingly, this reflects the incorporation of NH<sub>2</sub> groups, with emphasis on MS and CS. Comparing the IR spectra of sono-aminated chars with their %N content leads to the conclusion that MS, CS, WS and RS showed intensified nitrogenation. Thus, the FTIR spectrum also corroborate sono-amination resulted to attach more amines than amination alone that subsequently improve adsorption capacities of the activated chars.

# Figures 10-13

#### 3.5 Raman Analysis

The Raman spectra of raw and activated biochars under the different treatment conditions (ultrasonically activated, amine activated and sono-chemically activated) are demonstrated in Figures 14-17. Raman spectroscopy has been widely used to evaluate the microstructure of carbon materials, particularly the distribution and state of sp<sup>2</sup>-bonded (aromatic) carbon, which is embedded in a disordered and amorphous matrix of both sp<sup>3</sup> and sp<sup>2</sup> carbon [65]. Overall, the Raman spectra reveal the presence of an amorphous phase along with highly disordered graphiticlike crystallites in all char samples. The figures exhibit two prominent peaks around 1400 and 1600 cm<sup>-1</sup> which are assigned to the D-band and the G-band respectively. The D-band is attributed to in-plane vibrations of sp<sup>2</sup> bonded carbon (intramolecular C–C vibration of aromatic carbon layers) within structural defects [66]. The G-band arises from the in-plane vibrations of the sp<sup>2</sup>-bonded crystallite carbon (intermolecular shear vibration between individual C-layers) [67]. In addition, another band around 2800 cm<sup>-1</sup> can be observed which indicates the multilayer graphene-phase structure [68]. The ratio of the D to G bands (I<sub>D</sub>/I<sub>G</sub>), termed the intensity ratio, describes the graphitization degree of carbonaceous materials and is tabulated in Table 6 for all the samples [68]. The lower the  $I_D/I_G$  ratio, the higher the graphitization of a carbonaceous structure.

Effect of Feedstock Origin: As observed in Table 6, the raw samples intensity ratios ranged between 0.71-0.79 where rice straw had the highest (0.79) and miscanthus had the lowest value (0.71), with the following order for intensity ratios: crop residue (RS>RH>WS>SR) > agro industrial residue (SB>CS) > herbaceous residue (SG>MS). This can be explained in the following way: during formation of char, the biomass undergoes a first stage decomposition where a 3D network of benzene rings is formed with separate or bicyclic aromatic rings having functional groups such as methyl, methylene, oxygen etc. attached [69]. In the second stage, cleavage reactions occur (involving -OH, -COOH and -CO groups) that lead to increases in the number of fused aromatic rings, resulting in more-extended 2D structures [69]. The char formation finally ends up with the formation of microcrystalline structures consisting of greater than six fused aromatic rings [69]. This crystalline structure (with high carbon content) results in less disorder in biochars like herbaceous (MS, SG) and agro-industrial residues (CS, SB) that have higher %C content compared to crop residues, and accordingly they exhibit low intensity ratios. Additionally, literature suggests that the biochars with high cellulose and hemicellulose content and low lignin content like MS, SG, CS and SB possesses less disorder [70] and have lower intensity ratios (or higher graphitic structure) than biochars that possess high lignin content, like SR, WS, RH and RS.

Effect of ultrasound: According to the Table 6, the I<sub>D</sub>/I<sub>G</sub> ratios of the five raw biochars with the lowest intensity ratios increased upon sonication, implying the presence of more sp<sup>3</sup> bonds and more defects and disorders in sonicated samples. Physical activation led to a maximum enhancement of I<sub>D</sub>/I<sub>G</sub> ratio to 0.81 for MS, and the intensity ratios exhibited the following order: MS>SG=CS>SB>SR=WS>RH>RS. The surface areas of these chars followed the same trend, as ultrasonic cavitation exfoliated the biochar structures, followed by removal of mineral matter (ash)

and enhancement of surface area and pore volume. This resulted in the addition of disorder to the structure and therefore increased the I<sub>D</sub>/I<sub>G</sub> ratio. However, RH and RS showed reduced values of I<sub>D</sub>/I<sub>G</sub> ratio after sonication and WS has almost no change in intensity ratio. A reduction of intensity ratio can indicate an increase in aromaticity in biochars [71]. This can be further supported based on the elemental analysis result (Table 4) of these chars that show acoustic cavitation resulted in reduction of %N content for RH and RS whereas WS showed no change. This supports the observed trend for the I<sub>D</sub>/I<sub>G</sub> ratio of WS, RH and RS. Henceforth, based on the above discussion, it can be concluded that ultrasound resulted in a reduced degree of graphitization for herbaceous (MS, SG) and agro industrial (CS, SB) based chars as reflected in their higher intensity ratios, whereas crop residue chars showed higher graphitization degrees by their reduced intensity ratios. <u>Effect of amination:</u> The five raw biochars with the lowest intensity ratios showed increment upon amination; two chars had decreased ratios and one didn't show any change. The intensity ratios for chemically modified samples ranged between 0.69 and 0.83; these were 0.87-1.2 times those of the raw chars with the following trend: herbaceous residue: MS>SG; agro industrial residue: CS=SB; crop residues: SR>WS>RH>RS. This suggests that this is the trend of the extent of amination, since amination should cause defects. In addition to that, the extent of decrease in surface area (Table 3) upon amine functionalization also follows the same trend, as increased amination fills pores.

Effect of sono amination (compared to raw biochar): As observed, sono-chemical activation created more defects (in terms of intensity ratio) than raw samples had for 5 of the chars, and fewer defects for 2 of them. US-Am intensity ratios were 0.94-1.2 times those of raw chars, with the following trend: herbaceous residues > agro-industrial residues > crop residues, with the maximum and minimum ratios for MS (0.84) and RS (0.74), respectively. Moreover, the observed trend

further matched the textural analysis (Table 3) that showed sono-amination resulted in lower surface areas than raw chars as a result of amine grafting. Thus, the above discussion elucidates that MS, with increased %N content and lower surface area had additional defects in its structure and an increased intensity ratio, where RS, with low %N, showed a low intensity ratio.

Effect of sono amination (compared to aminated biochar): In comparison to aminated chars, increases in intensity ratios of sono-aminated chars followed the trend of: RS>SG>CS~MS (1.01-1.07 times aminated-only values) while SB, SR, WS and RH didn't show any change in their I<sub>D</sub>/I<sub>G</sub> ratio. As found in Table 4, MS showed increased %N content, suggesting modification of the biochar structure that would be associated with an increased intensity ratio; however, WS and RH significantly increased their %N without a concomitant change in intensity ratio. SB and SR had reduced %N content and so did not show an increase in intensity ratio. In spite of sono-aminated biochars having lower surface areas than aminated chars, the acoustic energy transferred during sono-chemical activation resulted in higher disorder in the biochars (through exfoliation and ash removal) and contributed to more defects. In accord, the FTIR spectra (Figures 24 and 25) showed that intensity of peaks at 1100-1200 cm<sup>-1</sup> (C-N) are strong for all sono-aminated chars, especially MS and CS, but are less intense for SB and SR, consistent with the high and low intensity ratios of these chars, respectively.

Hence, the above discussion reveals that sono-chemical activation played a more promising role for herbaceous (MS, SG) and agro industrial residues than for crop residues (SR, WS and RH) in terms of increasing  $I_D/I_G$  intensity ratios, which may imply improve subsequent  $CO_2$  removal capacity.

## Table 6, Figures 14-17

## 3.6 Adsorption Study

Effect of Feedstock Origin: Figure 18 presents adsorption capacities of different biochars under different activation conditions, and their corresponding breakthrough plots have been reported in supplementary documents Figures 26-29. As observed, raw biochar samples have adsorption capacities in the range of 0.49-0.82 mmol/g with the following order: herbaceous (MS and SG) > agro-industrial (CS and SB) > crop residues (SR, WS, RH and RS). This trend can be correlated to their ligninocellulosic compositions that exhibit high cellulose and low lignin for MS and SG chars, which accordingly possess high %C and surface area, since cellulose degrades preferentially over lignin. Despite high %N and comparable %C content of SG with respect to MS, SG has a lower adsorption capacity because of its higher ash content. Among agro-industrial residues, CS is found to have a higher adsorption capacity than SB. Although the carbon contents of these two biochars are comparable (Table 5), CS has higher %N and lower %ash content and also a larger surface area than SB. Crop residues have notably the lowest adsorption capacity of the biochar categories. SR and WS have very similar %C contents (Table 5), along with very close %ash and %N values. These observations are also in accordance with the surface area analyses and thus SR and WS exhibit similar adsorption capacity values. On the other hand, RH and RS showed very low values for adsorption capacity, consistent with their high ash content, low %C and low surface area.

The breakthrough plot for raw chars (Figure 26) describes the effluent adsorptive concentration at the outlet of the adsorption bed. The concentration wave moves through the bed as the adsorption proceeds and so most of the mass transfer at any one time occurs in a fairly small region. The mass transfer zone moves down the bed until it "breaks through" at the point where the adsorbent no longer will be solely adsorbed to the biochar (adsorbate) and starts to appear in the effluent. For herbaceous biochars MS and SG, the breakthrough curves shift to the right compared to the other

plots. This signifies that more adsorbate was adsorbed by the adsorbent and hence the adsorption capacity increased. Moving on to next category, agro-industrial chars have smaller shifts from the origin and so they have lesser adsorption capacities than herbaceous biochars, and similarly for crop residues.

Effect of Physical Activation on CO<sub>2</sub> Adsorption: Physical activation employing ultrasonication had a noticeable effect in improving adsorption capacities, in the range of 1.1-1.4 times the capacities of raw chars. The trend followed the pattern of the raw biochars, with MS exhibiting the highest and RS the lowest adsorption capacities. As Table 4 shows, sonicated MS and SG have relatively high %C and low %ash, and MS has a significant increment in nitrogen content; these properties support their highest adsorption behavior. Agro-industrial biochars also have improvement in %N, whereas crop residues (specifically RS) showed reduction (0.55 times) in %N, in accord with its smaller adsorption capacity. The change in the %N content of the biochars following ultrasonication, compared to raw chars, is in the same order as the adsorption ability: MS (0.3), SG (0.1), CS (0.1), SB (0.0), SR (-0.1), WS (-0.2), RH (-0.3), and RS (-1.4). This suggests that the nitrogen content that is increased or decreased by ultrasonication can assist in the adsorption of CO<sub>2</sub>. This shows the importance of nitrogen content for improving adsorption ability although why ultrasound should alter that type of nitrogen preferentially is not clear. Thus, based on the above discussion, it can be highlighted that ultrasonication resulted in improved %N content for MS, but showed negative affect for RH and RS, accounting for their high and low adsorption capacities respectively. Although sonication of SG, CS, SB, SR and WS didn't significantly change their %N contents, their adsorption capacities were higher than the corresponding raw chars; the capacities were higher than RH and RS but lower than MS.

Additionally, the breakthrough plots (Figure 27) reveal that herbaceous chars (MS, SG) and agroindustrial CS char had increased mass transfer zones with longer breakthrough times than the other sonicated chars, suggesting their superior adsorption capacities. The other agro-industrial and crop based biochars (SR, WS, RH, RS) had short breakthrough times, representing diminished adsorption capacity.

Effect of Amination on CO<sub>2</sub> Adsorption: Amine treated biochars exhibited 1.51-1.54 times higher adsorption capacities than raw biochar samples. The trend followed the pattern of the raw biochars. MS and RS showed the highest (1.27 mmol/g) and lowest (0.74 mmol/g) adsorption capacities, which is consistent with their micro and mesoporous surface areas and pore volumes. Amine functionalization resulted in increased %N of biochars in the range of 1.4 - 4 times. The %N content of the aminated chars had a negative correlation with their adsorption ability (except for RH). The order of %N contents (from Table 5) were: RS > WS > SR > SB > RH = CS = SG > MS. It may be that substantial portions of the %N of the poorly-adsorbing biochars are in groups, such as within aromatic rings, that do not interact well with CO<sub>2</sub>, or are sequestered in inaccessible locations. Breakthrough plots (Figure 28) further verified the above observed result of adsorption capacity of various aminated samples. MS, SG and CS had more prominent mass transfer zones, with more gradually sloping curves shifted towards the right, signifying increased adsorbate retention ability. SB, SR, WS, RH and RS had steep curves and short retention times, in concert with their lesser adsorption capacities.

<u>Effect of Sono-Amination on CO<sub>2</sub> Adsorption:</u> The integrated sono-chemical treatments resulted in increased adsorption capacities in the range of 2.8-3.1 times those of raw chars, with the trend following the pattern of the raw biochars. The effect of the applied physical activation during sono-amination can be observed in both micro and nano scale. Since biochar contains graphene cluster

so ultrasound induced microjets and shock waves expected to exfoliate the graphene cluster [24]. This effect can be corroborated by the Raman Spectroscopy that showed reduction trend of graphiticity and enhancement of distortion for the sonicated samples (Table 6). These structural alteration provides active sites for subsequent chemical modification using amine [23]. In addition to that the effect of acoustic treatment is also obvious in micro scale. Ultrasound cavitation and its consequences (shock waves and microjets) resulted to the generation of new pores/opening of blocked pores of the biochar which can be observed by SEM images (Figures 7-9) and further substantiated by the textural analysis (Table 3) that showed increased value of surface area and pore volume after sonication. Increased surface area and porosity can boost the physical adsoption of biochar while they may open channels to the under-layers. On the other hand, exfoliation of the graphitic structure of biochar exposes a greater number of potential groups to the amine functionalization. Thus, CO<sub>2</sub> capture capacity of biochar is not only determined by the enhanced surface area and pore volume but also by the basic amine functionalities which are the active sites for CO<sub>2</sub> adsorption [72, 73]. Indeed, the higher CO<sub>2</sub> uptake obtained for sono-aminated samples that have lower surface areas and pore volumes than the raw chars highlight the importance of the nitrogen functionalities on the surface of the modified adsorbents which can be further verified from elemental analysis that exhibit increased %N contents for ultrasonic-TEPA activated biochars. The similar findings were also reported in the literature [74]. As observed from tables (4-5) the treated chars had significant nitrogen increases (0.5-1.3 %N) compared to raw chars, although not necessarily with respect to amination-only chars. MS, with the most increased %N content, showed the most promising adsorption capacity. After MS, it can be observed that SG, CS and SB have a decreasing trend in surface area and pore volume followed by SR, WS and RS.

Despite good correlations of adsorption capacity to surface area, elemental analysis and Raman intensity ratios, correlations are poor when all treatment sets are considered together. This again suggests that a complex interplay of factors are involved in determining adsorption capacity. Furthermore, different factors may be in play for different biomass sources.

The sono-chemically treated chars had 1.8-2 times higher adsorption capacity than aminated-only chars. The breakthrough curves for MS, SG, and CS had increased mass transfer zones, followed by SB, SR, WS, RH and RS. Therefore, it can be concluded that sono-amination employing ultrasound and TEPA together can significantly improve the CO<sub>2</sub> adsorption capacities of biochar samples compared to either treatment alone. The dependence of adsorption capacity on biomass source followed the trend of herbaceous > agro-industrial > crop based biochars, with MS char having almost twice the adsorption capacity of RS char.

# Figure 18

#### 3.7 Mechanism of Physicochemical Activation of Char and Interactions with CO<sub>2</sub>

The interaction of char with acoustic cavitation and amine functionalization is represented in Figure 19. As observed from during the first step of the activation, the applied ultrasound waves promote cavitation that generates bubbles which result in high-speed liquid jets and shockwaves. This eventually drives into the surface of the biochar and increases the interlayer spacing among the layers. The ultrasound also causes vibration which passes through the biochar structure and gradually peels off the stacked graphene layers exposing the individual graphene sheets and the oxygen functional groups (–COOH, -OH and C=O). These functional groups helped to attach amine during chemical functionalization. However, -COOH group needs additional pre-activation using EDC-HOBt prior to amination. As found from the figure, EDC activates -COOH group to form O-acylisourea [75]. However, the reaction tends to produce N-acyl urea as undesired side

product and reducing the yield of the product by O-N migration of the activated carboxyl functional group which is prevented by adding additives such as HOBt that displaces EDC and forms the intermediate as shown in the Figure 19 [75]. In the final step, the nucleophilic attack by the amino group of TEPA resulted to form amide (–CONH) bond followed by release of HOBt as by product which can be easily removed through simple filtration

#### Figure 19

The major pathway that contributes to amine-based CO<sub>2</sub> capture includes the formations of carbamate anions for gas-solid reactions. During the reaction (Figure 20) at first amine molecules react with CO<sub>2</sub> molecule to form a carbamate ion and a protonated amine. This has been proposed to occur via two-step zwitterion mechanism. In the first step zwitterion is formed as intermediate through the interaction between terminal amino group and CO<sub>2</sub> followed by deprotonation in the second step by a base to produce a carbamate that resulted to the attachment of CO<sub>2</sub> with the aminated biochar structure (Scheme 1). Few literature reports that zwitterion is unstable to further proceed for CO<sub>2</sub> capture [76, 77]. However, more recently, ab initio molecular dynamics (AIMD) simulations based on density functional theory (DFT) demonstrates that reaction between CO<sub>2</sub> and amine occurs through two-step zwitterion mechanism [78]. Likewise, the terminal amino group, the reaction for intermediate amino group proceeds by nucleophilic addition of 1 mol of amine to the carbons of 1 mol of CO<sub>2</sub> forming 1 mol of ammonium-carbamate zwitterion intermediates as shown in Scheme 2. The zwitterions are then deprotonated by 1 mol of free amine groups, producing 1 mol of ammonium-carbamate ion pairs [79].

# Figure 20

#### 3.8 Regeneration Study

Stability analysis of the adsorbent is important from an economic point of view as well as for long term use. Figure 21 shows the cyclic adsorption-desorption behavior of different sono-chemically treated samples. As observed, after 15 cycles the adsorptive capacities were reduced in the range of 24-32% than the original adsorption capacities. The maximum and minimum reductions were observed for crop and herbaceous based biochars respectively. As found from the figure, herbaceous and agro-industrial biochars have comparable regeneration ability as these biochars retained 74-76% of their actual adsorption capacities after 15 cycles. Whereas the significant reduction in adsorption capacities (30-32%) were observed for crop residues. The greater the cyclic adsorption capacity, the lesser the replacement of the adsorbent and potentially more efficient the adsorbent will be. Thus, based on this point of view it is suggested that herbaceous and agro-industrial based biochars are more promising than crop residue based biochars in terms of both adsorption and regeneration behaviors.

The probable reason for the reduction of adsorption capacities could be the volatilization or loss of reactive amino functional groups from the aminated adsorbents [80]. Literature also shows that the interaction between CO<sub>2</sub> and amine above 403 K resulted in the formation of urea linkage followed by the loss of water [80]. This may occur either from the secondary reaction of the carbamate ion formed (R1) or direct reaction of CO<sub>2</sub> and the amine group (R2) [80]. Thus, formation and deposition of stable urea compounds on the surface of the adsorbent during thermal reactions tend to reduce the interaction between CO<sub>2</sub> and the amino functional groups that leads to the reduction of adsorption capacity [81]. Usually, the regeneration is carried out at very high temperatures, ranging from 200 to 500°C [82, 83]. However, in the present study was conducted under much lower temperature range of 453 K (180°C) to make the process less energy intensive and more economic.

$$RNH_3 + R_2NCOO$$
  $R_2NCONHR + H_2O$   $R_1$   $2R_2NH + CO_2$   $R_2NCONR_2 + H_2O$   $R_2$ 

Figure 21

#### 4 Conclusions

The current study investigated the effect of biomass origin on the carbonaceous structure (including its physical and chemical properties), activation conditions and CO<sub>2</sub> adsorption capacities of biochar that were prepared from eight different biomasses of three different categories: herbaceous, agro-industrial and crop residues. The biochars were subjected to acousticbased physical activation, chemical functionalization, and integrated physicochemical activation techniques. The biochar production is affected by the following factors-moisture, volatiles and mineral matter contents which are further controlled by biomass feedstock sources primarily cellulose, hemicellulose and lignin contents. Biochars produced from high cellulose and low lignin contents biomass have higher %C and reduced %ash contents as observed for herbaceous and agro industrial chars than crop based chars. Additionally, chars with the highest %C and lowest %ash contents interact very effectively with ultrasound with further enhancement of their carbon and ash contents. The advantages of the induced interactions between ultrasound and carbonaceous structure include enhancement of microporous surface area and micro-porosity. Micropores have higher surface area than meso or macropores because of the lowest pore size thus induced microporosity increases specific surface area of the char and making it effective for the subsequent amination and CO<sub>2</sub> adsorption. The results showed that the highest improvements of adsorption capacities were attained for the combined ultrasono-amine functionalization technique that increased adsorption between 184-200% over raw char. Among the different categories the herbaceous based biochars MS and SG have the highest adsorption capacities of 2.53 and 2.37

mmol/g respectively at 0.10 atm. and 70 °C. This is primarily attributed to the high %C content (77-82%), low %ash content (4.35-12.78) and improved textural properties (324-340 m²/g) which promoted enhanced nitrogenation during amination and facilitated CO<sub>2</sub> adsorption. Additionally, the entire sono-chemical activation is conducted at room temperature, which makes it very energy efficient, while utilization of easily-available biomass makes it highly economic, providing an efficient way for synthesizing adsorbent for effective CO<sub>2</sub> adsorption.

## Acknowledgements

The authors are grateful for the financial support of the National Science Foundation (NSF EPSCoR RII Grant No. OIA-1632899 and MRI Grant No. CHE-1532079). Various other supports from the University of Mississippi are also gratefully acknowledged. Scanning electron microscopy analyses presented in this work were conducted at the Microscopy and Imaging Center (SEM Core) of the University of Mississippi. This facility is supported in part by grant 1726880, National Science Foundation.

#### References

- 1. Stiasny, M.H., et al., Ocean acidification effects on Atlantic cod larval survival and recruitment to the fished population. PLoS One, 2016. 11(8): p. e0155448.
- 2. Hu, S., et al., Effect of CO<sub>2</sub>-induced seawater acidification on growth, photosynthesis and inorganic carbon acquisition of the harmful bloom-forming marine microalga, Karenia mikimotoi. PloS one, 2017. **12**(8): p. e0183289.
- 3. Koytsoumpa, E.I., C. Bergins, and E. Kakaras, *The CO<sub>2</sub> economy: Review of CO<sub>2</sub> capture and reuse technologies.* The Journal of Supercritical Fluids, 2018. **132**: p. 3-16.
- 4. Cai, J., et al., Review of physicochemical properties and analytical characterization of lignocellulosic biomass. Renewable and Sustainable Energy Reviews, 2017. **76**: p. 309-322.
- 5. Mimmo, T., et al., *Effect of pyrolysis temperature on miscanthus* (*Miscanthus* × *giganteus*) *biochar physical, chemical and functional properties*. Biomass and Bioenergy, 2014. **62**: p. 149-157.
- 6. Oliveira, J.A., et al., Comparison of Miscanthus and Switchgrass Cultivars for Biomass Yield, Soil Nutrients, and Nutrient Removal in Northwest Spain. Agronomy Journal, 2017. **109**: p. 122-130.

- 7. Sadaka, S., et al., *Characterization of biochar from switchgrass carbonization*. Energies, 2014. **7**(2): p. 548-567.
- 8. Janus, A., et al., Elaboration, characteristics and advantages of biochars for the management of contaminated soils with a specific overview on Miscanthus biochars. Journal of environmental management, 2015. **162**: p. 275-289.
- 9. Shen, Y., et al., *Producing pipeline-quality biomethane via anaerobic digestion of sludge amended with corn stover biochar with in-situ CO<sub>2</sub> removal.* Applied energy, 2015. **158**: p. 300-309.
- 10. Wang, Y., et al., *Porous carbonaceous materials from hydrothermal carbonization and KOH activation of corn stover for highly efficient CO<sub>2</sub> capture AU Shen, Feng. Chemical Engineering Communications, 2018. 205(4): p. 423-431.*
- 11. Luo, S., et al., *Preparation and characterization of amine-functionalized sugarcane bagasse for CO*<sub>2</sub> *capture*. Vol. 168. 2015. 142-148.
- 12. Sriprasoed, R., N. Patikarnmonthon, and K. Kamwilaisak, *Comparison study of sugarcane leaves and corn stover as a potential energy source in pyrolysis process*. Energy procedia, 2016. **100**: p. 26-29.
- 13. Janke, L., et al., *Biogas production from sugarcane waste: assessment on kinetic challenges for process designing.* International journal of molecular sciences, 2015. **16**(9): p. 20685-20703.
- 14. Mourtzinis, S., et al., *Carbohydrate and nutrient composition of corn stover from three southeastern USA locations*. Biomass and Bioenergy, 2016. **85**: p. 153-158.
- 15. Xu, X., et al., Chemical transformation of CO<sub>2</sub> during its capture by waste biomass derived biochars. Environmental pollution, 2016. **213**: p. 533-540.
- 16. Zhang, X., et al., Effects of hydrofluoric acid pre-deashing of rice husk on physicochemical properties and CO<sub>2</sub> adsorption performance of nitrogen-enriched biochar. Energy, 2015. **91**: p. 903-910.
- 17. Chuah, T.G., et al., *Rice husk as a potentially low-cost biosorbent for heavy metal and dye removal: an overview.* Desalination, 2005. **175**(3): p. 305-316.
- 18. Uzunova, S., et al., *Preparation of low-ash-content porous carbonaceous material from rice husks*. Bulg. Chem. Commun, 2010. **42**(2): p. 130-137.
- 19. Manna, S. and N. Singh, *Effect of wheat and rice straw biochars on pyrazosulfuron-ethyl sorption and persistence in a sandy loam soil.* Journal of Environmental Science and Health, Part B, 2015. **50**(7): p. 463-472.
- 20. Sajjadi, B., W.-Y. Chen, and N.O. Egiebor, *A comprehensive review on physical activation of biochar for energy and environmental applications*. Reviews in Chemical Engineering, 2019. **35**(6): p. 735-776.
- 21. Hagemann, N., et al., *Activated carbon, biochar and charcoal: linkages and synergies across pyrogenic carbon's ABCs.* Water, 2018. **10**(2): p. 182.

- 22. Sajjadi, B., W.-Y. Chen, and O. Egiebor Nosa, *A comprehensive review on physical activation of biochar for energy and environmental applications*, in *Reviews in Chemical Engineering*. 2018.
- 23. Guittonneau, F., et al., *The effect of high power ultrasound on an aqueous suspension of graphite*. Ultrasonics Sonochemistry, 2010. **17**(2): p. 391-398.
- 24. Stankovich, S., et al., *Graphene-based composite materials*. Nature, 2006. **442**: p. 282.
- 25. Chen, W.Y., et al., *Photochemical and acoustic interactions of biochar with CO2 and H2O: applications in power generation and CO<sub>2</sub> capture.* AIChE Journal, 2014. **60**(3): p. 1054-1065.
- 26. Sajjadi, B., et al., *Variables governing the initial stages of the synergisms of ultrasonic treatment of biochar in water with dissolved CO*<sub>2</sub>. Fuel, 2019. **235**: p. 1131-1145.
- 27. Munoz, D.M., et al., *New liquid absorbents for the removal of CO<sub>2</sub> from gas mixtures*. Energy & Environmental Science, 2009. **2**(8): p. 883-891.
- 28. Dondini, M., et al., *The potential of Miscanthus to sequester carbon in soils: comparing field measurements in Carlow, Ireland to model predictions.* Gcb Bioenergy, 2009. **1**(6): p. 413-425.
- 29. Oliveira, J.A., et al., Comparison of miscanthus and switchgrass cultivars for biomass yield, soil nutrients, and nutrient removal in northwest spain. Agronomy Journal, 2017. **109**(1): p. 122-130.
- 30. Xiaofeng, B., et al., *Properties and applications of biochars derived from different biomass feedstock sources*. International Journal of Agricultural and Biological Engineering, 2017. **10**(2): p. 242-250.
- 31. Chatterjee, R., et al., *Ultrasound cavitation intensified amine functionalization: A feasible strategy for enhancing CO<sub>2</sub> capture capacity of biochar.* Fuel, 2018. **225**: p. 287-298.
- 32. Chatterjee, R., et al., Low Frequency Ultrasound Enhanced Dual Amination of Biochar: A Nitrogen-Enriched Sorbent for CO2 Capture. Energy & fuels, 2019. **33**(3): p. 2366-2380.
- 33. Hamdaoui, O., et al., *Effects of ultrasound on adsorption—desorption of p-chlorophenol on granular activated carbon*. Ultrasonics Sonochemistry, 2003. **10**(2): p. 109-114.
- 34. Sellaperumal, P., *Evaluation of thermochemical decomposition of various lignocellulosic biomasses for biochar production.* 2012: McGill University (Canada).
- 35. Chemerys, V. and E. Baltrėnaitė, *A review of lignocellulosic biochar modification towards enhanced biochar selectivity and adsorption capacity of potentially toxic elements*. Ukrainian Journal of Ecology, 2018. **8**(1): p. 21-32.
- 36. Li, J., et al., A comparison of biochars from lignin, cellulose and wood as the sorbent to an aromatic pollutant. Journal of hazardous materials, 2014. **280**: p. 450-457.
- 37. Chatterjee, R., et al., *Ultrasound cavitation intensified amine functionalization: A feasible strategy for enhancing CO 2 capture capacity of biochar.* Fuel, 2018. **225**: p. 287-298.
- 38. Chatterjee, R., et al., Low Frequency Ultrasound Enhanced Dual Amination of Biochar: A Nitrogen-Enriched Sorbent for CO<sub>2</sub> Capture. Energy & Fuels, 2019.

- 39. Zhou, M., J. Yu, and B. Cheng, *Effects of Fe-doping on the photocatalytic activity of mesoporous TiO*<sub>2</sub> *powders prepared by an ultrasonic method.* Journal of Hazardous Materials, 2006. **137**(3): p. 1838-1847.
- 40. Houshmand, A., W.M.A. Wan Daud, and M.S. Shafeeyan, *Exploring Potential Methods* for Anchoring Amine Groups on the Surface of Activated Carbon for CO<sub>2</sub> Adsorption. Separation Science and Technology, 2011. **46**(7): p. 1098-1112.
- 41. Huang, Z.-H., et al., Relation between the charge efficiency of activated carbon fiber and its desalination performance. Langmuir, 2012. **28**(11): p. 5079-5084.
- 42. Teng, Y., et al., *Promoting Effect of Inorganic Alkali on Carbon Dioxide Adsorption in Amine-Modified MCM-41*. Energies, 2016. **9**(9): p. 667.
- 43. Yue, M.B., et al., Efficient CO<sub>2</sub> capturer derived from as synthesized MCM 41 modified with amine. Chemistry—A European Journal, 2008. **14**(11): p. 3442-3451.
- 44. Brunauer, S., et al., *On a theory of the van der Waals adsorption of gases*. Journal of the American Chemical society, 1940. **62**(7): p. 1723-1732.
- 45. PatriciaOrdonez, S., C.H. García, and J. Larrahondo, *Fruit Waste and Sugarcane Bagasse as Potential Natural Resources of Mineral and Lipophilic Substances*.
- 46. Xu, G., et al., What is more important for enhancing nutrient bioavailability with biochar application into a sandy soil: Direct or indirect mechanism? Ecological engineering, 2013. **52**: p. 119-124.
- 47. Brewer, C.E., et al., *Characterization of biochar from fast pyrolysis and gasification systems*. Environmental Progress & Sustainable Energy: An Official Publication of the American Institute of Chemical Engineers, 2009. **28**(3): p. 386-396.
- 48. Wu, W., et al., *Chemical characterization of rice straw-derived biochar for soil amendment.* Biomass and bioenergy, 2012. **47**: p. 268-276.
- 49. Singh, B., B.P. Singh, and A.L. Cowie, *Characterisation and evaluation of biochars for their application as a soil amendment.* Soil Research, 2010. **48**(7): p. 516-525.
- 50. Paiva, C.L., et al., *Mineral content of sorghum genotypes and the influence of water stress.* Food Chemistry, 2017. **214**: p. 400-405.
- 51. Sajjadi, B., W.-Y. Chen, and N.O. Egiebor, *A comprehensive review on physical activation of biochar for energy and environmental applications*. Reviews in Chemical Engineering, 2018.
- 52. Zhou, Y., et al., Sorption of heavy metals on chitosan-modified biochars and its biological effects. Chemical Engineering Journal, 2013. **231**: p. 512-518.
- 53. Chen, B., D. Zhou, and L. Zhu, *Transitional adsorption and partition of nonpolar and polar aromatic contaminants by biochars of pine needles with different pyrolytic temperatures*. Environmental science & technology, 2008. **42**(14): p. 5137-5143.
- 54. Krukowski, E.G., et al., *FT-IR study of CO<sub>2</sub> interaction with Na+ exchanged montmorillonite*. Applied Clay Science, 2015. **114**: p. 61-68.

- 55. Xu, S., et al., *Alkali-assisted hydrothermal route to control submicron-sized nanoporous carbon spheres with uniform distribution*. Colloids and Surfaces A: Physicochemical and Engineering Aspects, 2017. **515**: p. 1-11.
- 56. Das, O., A.K. Sarmah, and D. Bhattacharyya, *A novel approach in organic waste utilization through biochar addition in wood/polypropylene composites*. Waste Management, 2015. **38**: p. 132-140.
- 57. Peterson, S.C., et al., Comparing corn stover and switchgrass biochar: characterization and sorption properties. Journal of agricultural science, 2013. **5**(1): p. 1.
- 58. Kim, W.-K., et al., Characterization of cadmium removal from aqueous solution by biochar produced from a giant Miscanthus at different pyrolytic temperatures. Bioresource technology, 2013. **138**: p. 266-270.
- 59. Liu, Y., Z. He, and M. Uchimiya, Comparison of biochar formation from various agricultural by-products using FTIR spectroscopy. Modern Applied Science, 2015. **9**(4): p. 246.
- 60. Coates, J., *Interpretation of infrared spectra, a practical approach*. Encyclopedia of analytical chemistry: applications, theory and instrumentation, 2006.
- 61. Vaughn, S.F., et al., Comparison of biochars derived from wood pellets and pelletized wheat straw as replacements for peat in potting substrates. Industrial crops and products, 2013. **51**: p. 437-443.
- 62. Fuertes, A., et al., Chemical and structural properties of carbonaceous products obtained by pyrolysis and hydrothermal carbonisation of corn stover. Soil Research, 2010. **48**(7): p. 618-626.
- 63. Lee, T., R. Othman, and F.-Y. Yeoh, *Development of photoluminescent glass derived from rice husk.* 2013.
- 64. Udvardi, B., et al., Effects of particle size on the attenuated total reflection spectrum of minerals. Applied spectroscopy, 2017. **71**(6): p. 1157-1168.
- 65. Zhao, L., et al., *Heterogeneity of biochar properties as a function of feedstock sources and production temperatures.* Journal of hazardous materials, 2013. **256**: p. 1-9.
- 66. Paris, O., C. Zollfrank, and G.A. Zickler, *Decomposition and carbonisation of wood biopolymers—a microstructural study of softwood pyrolysis*. Carbon, 2005. **43**(1): p. 53-66.
- 67. Lespade, P., R. Al-Jishi, and M. Dresselhaus, *Model for Raman scattering from incompletely graphitized carbons*. Carbon, 1982. **20**(5): p. 427-431.
- 68. Sajjadi, B., et al., *Urea functionalization of ultrasound-treated biochar: A feasible strategy for enhancing heavy metal adsorption capacity.* Ultrasonics Sonochemistry, 2019. **51**: p. 20-30.
- 69. Yang, H., et al., *Biomass-based pyrolytic polygeneration system for bamboo industry waste: evolution of the char structure and the pyrolysis mechanism.* Energy & Fuels, 2016. **30**(8): p. 6430-6439.

- 70. Tsaneva, V., et al., Assessment of the structural evolution of carbons from microwave plasma natural gas reforming and biomass pyrolysis using Raman spectroscopy. Carbon, 2014. **80**: p. 617-628.
- 71. Mohanty, P., et al., Evaluation of the physiochemical development of biochars obtained from pyrolysis of wheat straw, timothy grass and pinewood: effects of heating rate. Journal of analytical and applied pyrolysis, 2013. **104**: p. 485-493.
- 72. Drage, T.C., et al., *Preparation of carbon dioxide adsorbents from the chemical activation of urea–formaldehyde and melamine–formaldehyde resins.* Fuel, 2007. **86**(1-2): p. 22-31.
- 73. Shafeeyan, M.S., et al., *Ammonia modification of activated carbon to enhance carbon dioxide adsorption: effect of pre-oxidation.* Applied Surface Science, 2011. **257**(9): p. 3936-3942.
- 74. Zhang, C., et al., *CO2 capture with activated carbon grafted by nitrogenous functional groups*. Energy & fuels, 2013. **27**(8): p. 4818-4823.
- 75. Valeur, E. and M. Bradley, *Amide bond formation: beyond the myth of coupling reagents*. Chemical Society Reviews, 2009. **38**(2): p. 606-631.
- 76. Da Silva, E.F. and H.F. Svendsen, *Ab initio study of the reaction of carbamate formation from CO2 and alkanolamines*. Industrial & engineering chemistry research, 2004. **43**(13): p. 3413-3418.
- 77. Da Silva, E.F. and H.F. Svendsen, *Computational chemistry study of reactions, equilibrium and kinetics of chemical CO2 absorption.* International Journal of Greenhouse Gas Control, 2007. **1**(2): p. 151-157.
- 78. Stowe, H.M. and G.S. Hwang, Fundamental Understanding of CO2 Capture and Regeneration in Aqueous Amines from First-Principles Studies: Recent Progress and Remaining Challenges. Industrial & Engineering Chemistry Research, 2017. **56**(24): p. 6887-6899.
- 79. Wilfong, W.C., C.S. Srikanth, and S.S. Chuang, *In situ ATR and DRIFTS studies of the nature of adsorbed CO2 on tetraethylenepentamine films*. ACS applied materials & interfaces, 2014. **6**(16): p. 13617-13626.
- 80. Drage, T.C., et al., *Thermal stability of polyethylenimine based carbon dioxide* adsorbents and its influence on selection of regeneration strategies. Microporous and Mesoporous Materials, 2008. **116**(1): p. 504-512.
- 81. Ezeh, C.I., et al., Sonochemical surface functionalization of exfoliated LDH: Effect on textural properties, CO2 adsorption, cyclic regeneration capacities and subsequent gas uptake for simultaneous methanol synthesis. Ultrasonics Sonochemistry, 2017. **39**: p. 330-343.
- 82. Song, X., et al., Regeneration performance and mechanism of modified walnut shell biochar catalyst for low temperature catalytic hydrolysis of organic sulfur. Chemical Engineering Journal, 2017. **330**: p. 727-735.

- 83. Lashaki, M.J., et al., Effect of Adsorption and Regeneration Temperature on Irreversible Adsorption of Organic Vapors on Beaded Activated Carbon. Environmental Science & Technology, 2012. **46**(7): p. 4083-4090.
- 84. Brosse, N., et al., *Miscanthus: a fast-growing crop for biofuels and chemicals production.* Biofuels, Bioproducts and Biorefining, 2012. **6**(5): p. 580-598.
- 85. Bajpai, P., *Structure of Lignocellulosic Biomass*. SpringerBriefs in Molecular Science. 2016, Singapore: Springer.
- 86. Saeed, H.A., et al., Evaluation of Sudanese Sorghum and Bagasse as a Pulp and Paper Feedstock. BioResources, 2017. **12**(3): p. 5212-5222.
- 87. Anwar, Z., M. Gulfraz, and M. Irshad, *Agro-industrial lignocellulosic biomass a key to unlock the future bio-energy: a brief review.* Journal of radiation research and applied sciences, 2014. 7(2): p. 163-173.
- 88. Burhenne, L., et al., *The effect of the biomass components lignin, cellulose and hemicellulose on TGA and fixed bed pyrolysis*. Journal of Analytical and Applied Pyrolysis, 2013. **101**: p. 177-184.
- 89. Johar, N., I. Ahmad, and A. Dufresne, *Extraction, preparation and characterization of cellulose fibres and nanocrystals from rice husk*. Industrial Crops and Products, 2012. **37**(1): p. 93-99.
- 90. Nasri-Nasrabadi, B., T. Behzad, and R. Bagheri, *Extraction and characterization of rice straw cellulose nanofibers by an optimized chemomechanical method*. Journal of Applied Polymer Science, 2014. **131**(7).
- 91. Wilk, M. and A. Magdziarz, *Hydrothermal carbonization, torrefaction and slow pyrolysis of Miscanthus giganteus*. Energy, 2017. **140**: p. 1292-1304.
- 92. Peterson, S.C., et al., Comparing corn stover and switchgrass biochar: characterization and sorption properties. Journal of agricultural science, 2012. **5**(1): p. 1.
- 93. Imam, T. and S. Capareda, *Characterization of bio-oil, syn-gas and bio-char from switchgrass pyrolysis at various temperatures*. Journal of Analytical and Applied Pyrolysis, 2012. **93**: p. 170-177.
- 94. Sadaka, S., et al., *Characterization of biochar from switchgrass carbonization*. Energies, 2014. **7**(2): p. 548-567.
- 95. Hu, Z., et al., *Chemical profiles of switchgrass*. Bioresource technology, 2010. **101**(9): p. 3253-3257.
- 96. Clay, S.A., et al., *Maize, switchgrass, and ponderosa pine biochar added to soil increased herbicide sorption and decreased herbicide efficacy.* Journal of Environmental Science and Health, Part B, 2016. **51**(8): p. 497-507.
- 97. Mullen, C.A., et al., *Bio-oil and bio-char production from corn cobs and stover by fast pyrolysis*. Biomass and bioenergy, 2010. **34**(1): p. 67-74.
- 98. Carpenter, D.L., et al., *Pilot-scale gasification of corn stover, switchgrass, wheat straw, and wood: 1. Parametric study and comparison with literature.* Industrial & Engineering Chemistry Research, 2010. **49**(4): p. 1859-1871.

- 99. Rafiq, M.K., et al., *Influence of pyrolysis temperature on physico-chemical properties of corn stover (Zea mays L.) biochar and feasibility for carbon capture and energy balance*. PloS one, 2016. **11**(6): p. e0156894.
- 100. Lizotte, P.-L., P. Savoie, and A. De Champlain, *Ash content and calorific energy of corn stover components in Eastern Canada*. Energies, 2015. **8**(6): p. 4827-4838.
- 101. jutakridsada, P., et al., Comparison Study of Sugarcane Leaves and Corn Stover as a Potential Energy Source in Pyrolysis Process. Energy Procedia, 2016. **100**: p. 26-29.
- 102. Sun, Y., et al., *Effects of feedstock type, production method, and pyrolysis temperature on biochar and hydrochar properties.* Chemical Engineering Journal, 2014. **240**: p. 574-578.
- 103. Guimarães, J., et al., *Characterization of banana, sugarcane bagasse and sponge gourd fibers of Brazil.* Industrial Crops and Products, 2009. **30**(3): p. 407-415.
- 104. Inyang, M., et al., *Biochar from anaerobically digested sugarcane bagasse*. Bioresource Technology, 2010. **101**(22): p. 8868-8872.
- 105. Peng, Y. and S. Wu, *Fast pyrolysis characteristics of sugarcane bagasse hemicellulose*. Cellulose chemistry and technology, 2011. **45**(9): p. 605.
- 106. Naik, D.K., et al., *Pyrolysis of sorghum bagasse biomass into bio-char and bio-oil products*. Journal of Thermal Analysis and Calorimetry, 2017. **127**(2): p. 1277-1289.
- 107. Yin, R., et al., Characterization of bio-oil and bio-char obtained from sweet sorghum bagasse fast pyrolysis with fractional condensers. Fuel, 2013. 112: p. 96-104.
- 108. Santos, B.S. and S.C. Capareda, *Energy sorghum pyrolysis using a pressurized batch reactor*. Biomass Conversion and Biorefinery, 2016. **6**(3): p. 325-334.
- 109. Liu, Z., et al., Effect of the carbonization temperature on the properties of biochar produced from the pyrolysis of crop residues. BioResources, 2018. **13**(2): p. 3429-3446.
- 110. Ibrahim, N., et al., *Influence of reaction temperature and water content on wheat straw pyrolysis*. World Academy of Science, Engineering and Technology, International Journal of Chemical, Molecular, Nuclear, Materials and Metallurgical Engineering, 2012. **6**(10): p. 919-925.
- 111. Bruun, E.W., et al., *Effects of slow and fast pyrolysis biochar on soil C and N turnover dynamics*. Soil Biology and Biochemistry, 2012. **46**: p. 73-79.
- 112. Leng, L., et al., Surface characterization of rice husk bio-char produced by liquefaction and application for cationic dye (Malachite green) adsorption. Fuel, 2015. **155**: p. 77-85.
- 113. Ahiduzzaman, M. and A.K.M. Sadrul Islam, *Preparation of porous bio-char and activated carbon from rice husk by leaching ash and chemical activation*. SpringerPlus, 2016. **5**(1): p. 1248-1248.

Table 1. Lignino-cellulosic compositions of Different Biomasses

Biomass	Cellulose (wt.%)	Hemicellulose (wt.%)	Lignin (wt.%)	Ref
MS	40-60	20-40	10	[84]
SG	45	31.4	12	[85]
CS	38	26	19	[84, 86]
SB	42	25	20	[87]
SR	35.4	19.4	10.3	[86]
WS	38	29	15	[88]
RH	35	33	23	[89]
RS	32.1	24	18	[90]

Note: CS: Corn Stover; RH: Rice Husk; SB: Sugarcane Bagasse; SR: Sorghum; MS: Miscanthus; RS: Rice Straw; SG: Switch Grass; WS: Wheat Straw

**Table 2.** Physicochemical Properties of Different Biochars obtained from Literatures

Biochar	Pyrolys: Temper: ure (°C	at C, %	Н, %	0,%	N, %	S, %	Ash, %	Surface Area (m²/g)	pН	Ref.
MS	600	46.34-90	2.26- 5.88	6.7-47.62	0.31-0.33	0.09	2.25	381.5	10.0 5	[5, 8, 58, 91]
SG	600	82	2.4	14	1.2	0.3	4.6	188-260	9.1- 11.2	[92-96]
CS	600	52.8- 57.29	2.86	5.45	1.47	0.15	7.7-12	3.1	9.8	[9, 97- 101]
SB	600	45-46%	6.25	47.18	0.36	-	19.44	14.07	9.2	[102-105]
SR	550	49.3	2.65	24.28	0.91	0.04	18.78	-	-	[106-108]
WS	575	49.3	2.31	37.74	0.97	-	21.7	20.2	9.84	[15, 109- 111]
RH	650	42.04	5.28	30.64	0.38	0.17	33.36	1.5	5.62	[16, 109, 112, 113]
RS	600	38.62	6.1	10.71	1.3	_	13.77	25.6	6.5	[109]

**Table 3.** Surface Area Analysis of Different Biochar Samples (Raw, Ultrasonically, Chemically and Sono-Chemically Activated Biochars)

	Micro <sup>a</sup> -Porosity		Meso <sup>b</sup> Porosit	y
Sample Name	Surface area (m²/g)	Pore Volume (cm <sup>3</sup> /g)	Surface area (m²/g)	Pore Volume (cm <sup>3</sup> /g)
		Raw Biochars		
R-MS*	340	0.12	64	0.05
R-SG	324	0.11	61	0.05
R-CS	266	0.10	58	0.04
R-SB	220	0.10	40	0.03
R-SR	203	0.09	41	0.03
R-WS	179	0.07	39	0.03
R-RH	173	0.07	35	0.03
R-RS	152	0.06	33	0.03
	Ultraso	onically Treated C	hars	
US-MS!	520	0.17	61	0.04
US-SG	486	0.14	58	0.04
US-CS	399	0.14	55	0.04
US-SB	341	0.12	37	0.03
US-SR	320	0.11	36	0.03
US-WS	307	0.10	32	0.03
US-RH	281	0.10	30	0.03
US-RS	242	0.08	22	0.02

Aminated Chars						
Am-MS <sup>#</sup>	170	0.07	50	0.04		
Am -SG	169	0.07	42	0.03		
Am -CS	158	0.06	40	0.03		
Am -SB	109	0.04	28	0.03		
Am -SR	112	0.04	28	0.03		
Am -WS	111	0.04	25	0.02		
Am -RH	92	0.02	27	0.02		
Am -RS	90	0.02	22	0.02		
	Sono-Che	mically Treated Ch	ars			
US-Am-MS	207	0.09	39	0.03		
US-Am -SG	210	0.09	43	0.03		
US-Am -CS	170	0.07	42	0.03		
US-Am -SB	150	0.06	26	0.03		
US-Am -SR	138	0.06	28	0.03		
US-Am -WS	116	0.04	29	0.03		
US-Am -RH	107	0.04	23	0.02		
US-Am -RS	106	0.04	23	0.02		

<sup>\*</sup> R-raw; <sup>!</sup> US-ultrasound; <sup>#</sup> Am- amine, <sup>a</sup> micropores: d<2 nm and <sup>b</sup> mesopores: 2nm<d<50 nm

**Table 4.** Elemental compositions (dry basis) of Different Biochar Samples (Raw, Ultrasonically, Chemically and Sono-Chemically Activated Biochars)

Sample	C content (% wt.)	H content (% wt.)	N content (% wt.)	O content (% wt.)	S content (% wt.)	Ash content (% wt.)	pН		
Raw Biochars									
R-MS	82.35	2.32	0.28	11.22	0.03	4.35	8.77		
R-SG	77.00	2.04	0.57	9.68	0.03	12.78	10.56		
R-CS	74.47	2.24	0.81	11.82	0.09	12.00	11.56		
R-SB	68.10	1.90	0.49	10.08	0.03	19.78	9.48		
R-SR	67.76	1.87	1.09	10.51	0.09	18.84	11.72		
R-WS	66.18	1.60	1.27	9.92	0.13	23.16	11.54		
R-RH	49.30	1.67	0.32	10.10	0.02	40.15	9.91		
R-RS	50.17	1.49	1.41	9.57	0.23	38.68	11.06		
		Ultra	sonically Tre	ated Chars					
US-MS	86.91↑↑	1.99↓	0.55↑	6.65↓↓	0.03	3.73↓	•		
US-SG	79.67↑	0.87	0.64~	5.74	0.08	12.42↓			
US-CS	72.28↓	2.64↑	0.90~	14.51↑	0.09	10.88↓			
US-SB	73.39↑↑	1.75↓	0.50~	7.19↓	0.05	18.57↓			
US-SR	<b>74.31</b> ↑↑	1.87~	1.04~	7.47↓↓	0.04	15.52↓↓			
US-WS	81.35↑↑	1.73↑	1.27~	6.53↓↓	0.08	9.09↓↓			
US-RH	65.36↑↑	1.97↑	0.18	11.22↑	0.05	23.95↓↓			
US-RS	57.75↑↑	2.32↑	0.64↓	22.81 ↑↑	0.01	20.10↓↓			
		Am	inated Chars	1					
Am-MS	82.44~	2.49↑	1.12↑	11.02	0.03	3.31↓			

Am-SG	78.00↑	2.16↑	1.30↑	9.74~	0.06	7.84↓↓	
Am-CS	72.81	2.06↓	1.16	9.57↓	0.02	9.10↓	
Am-SB	68.87↑	1.93~	1.31↑	9.74↓	0.03	18.82↓	
Am-SR	71.78 <b>↑↑</b>	2.10	1.83↑	10.71↑	0.06	15.60↓↓	
Am-WS	67.85↑	1.77↑	1.89↑	10.53↑	0.08	19.29↓↓	
Am-RH	51.18↑	1.62~	0.89↑	9.61↓	0.01	38.55↓	
Am-RS	52.15↑	1.71↑	2.31↑	9.85↑	0.08	35.69↓	
		Sono-Che	emically Trea	ted Chars			
US-Am-MS	70.16↓↓↓↓	2.13↓↓	1.5↑↑	10.09↓↓	0.03	17.47↑↑↑	
US- Am-SG	69.71	2.06~↓	1.25 \( \sigma \)	10.37↑↑	0.09	17.38	
US-Am-CS	77.00 <mark>↑</mark> ↑↑	2.57↑↑	1.41↑↑	10.92↓↑	0.06	$7.90 \downarrow \downarrow \downarrow$	
US-Am-SB	78.11 <b>↑↑</b> ↑↑	2.24	1.12↑↓	10.15~↑	0.03	8.91	
US-Am-SR	81.12 <b>↑↑</b> ↑↑	2.60↑↑	1.25↑↓	12.80	0.02	$3.17 \downarrow \downarrow \downarrow \downarrow$	
US-Am-WS	53.58	1.81 \( \sim \)	2.10↑↑	8.48↓↓	0.10	$36.00\uparrow\uparrow\uparrow\uparrow$	
US-Am-RH	71.45 <b>↑</b> ↑↑	2.27↑↑	1.96↑↑	11.52↑↑	0.09	15.64 🙏 🗼	
US-Am-RS	52.09↑~	1.75↑~	2.25 \( \sim \)	9.22↓↓	0.10	37.34↓↓	

Note:  $\uparrow$  increase (0.1-3%);  $\downarrow$  decrease (0.1-3%); doubled arrows, significant change (> 3%),  $\sim$  not significant change (<0.1%),  $\blacksquare$  compared to raw BC,  $\blacksquare$  compared to aminated BC.

**Table 5.** Organic compositions (dry ash free basis) of Different Biochar Samples (Raw, Ultrasonically, Chemically and Sono-Chemically Activated Biochars)

Sample	C content (% wt.)	H content (% wt.)	N content (% wt.)	O content (% wt.)	S content (% wt.)	C/N		
Raw Biochars								
R-MS	85.6	2.4	0.3	11.7	0.03	343		
R-SG	86.2	2.3	0.6	10.8	0.03	158		
R-CS	83.3	2.5	0.9	13.2	0.10	107		
R-SB	84.5	2.4	0.6	12.5	0.04	162		
R-SR	83.3	2.3	1.3	12.9	0.11	73		
R-WS	83.7	2.0	1.6	12.5	0.16	61		
R-RH	80.3	2.7	0.5	16.4	0.03	180		
R-RS	79.8	2.4	2.2	15.2	0.37	42		
		Ultrasonic	ally Treated	Chars				
US-MS	90.4↑↑	2.1↓	0.6	6.9↓↓	0.03	184		
US-SG	91.6↑↑	1.0↓	0.7↑	6.6↓↓	0.09	145		
US-CS	79.9↓↓	2.9↑	1.0↑	16.1↑	0.10	94		
US-SB	88.5↑↑	2.1↓	0.6~	8.7↓↓	0.06	171		
US-SR	87.7↑↑	2.2↓	1.2↓	8.8↓↓	0.05	83		
US-WS	89.4↑↑	1.9↓	1.4↓	7.2↓↓	0.09	75		
US-RH	83.0↑	2.5↓	0.2↓	14.2↓	0.06	424		
US-RS	69.1↓↓	2.8↑	0.8↓	27.3↑↑	0.01	105		

	Aminated Chars						
Am-MS	84.9↓	2.6↑	1.2↑	11.3↓	0.03	86	
Am-SG	85.5	2.4↑	1.4	10.7	0.07	70	
Am-CS	85.0↑	2.4	1.4↑	11.2	0.02	73	
Am-SB	84.1	2.4~	1.6↑	11.9	0.04	61	
Am-SR	83.0	2.4↑	2.1	12.4	0.07	46	
Am-WS	82.6	2.2	2.3↑	12.8	0.10	42	
Am-RH	80.8	2.6	1.4↑	15.2	0.02	67	
Am-RS	78.9	2.6↑	3.5↑	14.9	0.12	26	
		Sono-Che	mically Tre	ated Chars			
US-Am-MS	83.6↓↓	2.5↑↑	1.8↑↑	12.0↑↑	0.04	55	
US- Am-SG	83.5↓↓	2.5↑↑	1.5↑↑	12.4↑↑	0.11	65	
US-Am-CS	83.7↑↓	2.8↑↑	1.5↑↑	11.9↓↑	0.07	64	
US-Am-SB	85.2↑↑	2.4~ ~	1.2↑↓	11.1↓↓	0.03	81	
US-Am-SR	83.0 \~	2.7↑↑	1.3~↓	13.1↑↑	0.02	76	
US-Am-WS	81.1↓↓	2.7↑↑	3.2↑↑	12.8 ↑ ~	0.15	30	
US-Am-RH	81.9↑↑	2.6↓~	2.2↑↑	13.2↓↓↓	0.10	43	
US-Am-RS	79.6↓↑	2.7↑↑	3.4↑↓	14.1↓↓	0.15	27	

**Note:** ↑ increase (0.1-3%); ↓ decrease (0.1-3%); doubled arrows, significant change (> 3%), ~ not significant change (<0.1%), ■ compared to raw BC, ■ compared to aminated BC.

Table 6. Raman Intensity Ratios of biochars samples (raw and activated under different conditions)

Sample Name	Raw	Physical Activation	Chemical Activation	Sono-chemical Activation
MS	0.71	0.81	0.83	0.84
SG	0.74	0.79	0.81	0.83
CS	0.74	0.79	0.81	0.82
SB	0.75	0.78	0.81	0.81
SR	0.75	0.77	0.79	0.79
WS	0.78	0.77	0.78	0.78
RH	0.78	0.73	0.75	0.75
RS	0.79	0.68	0.69	0.74

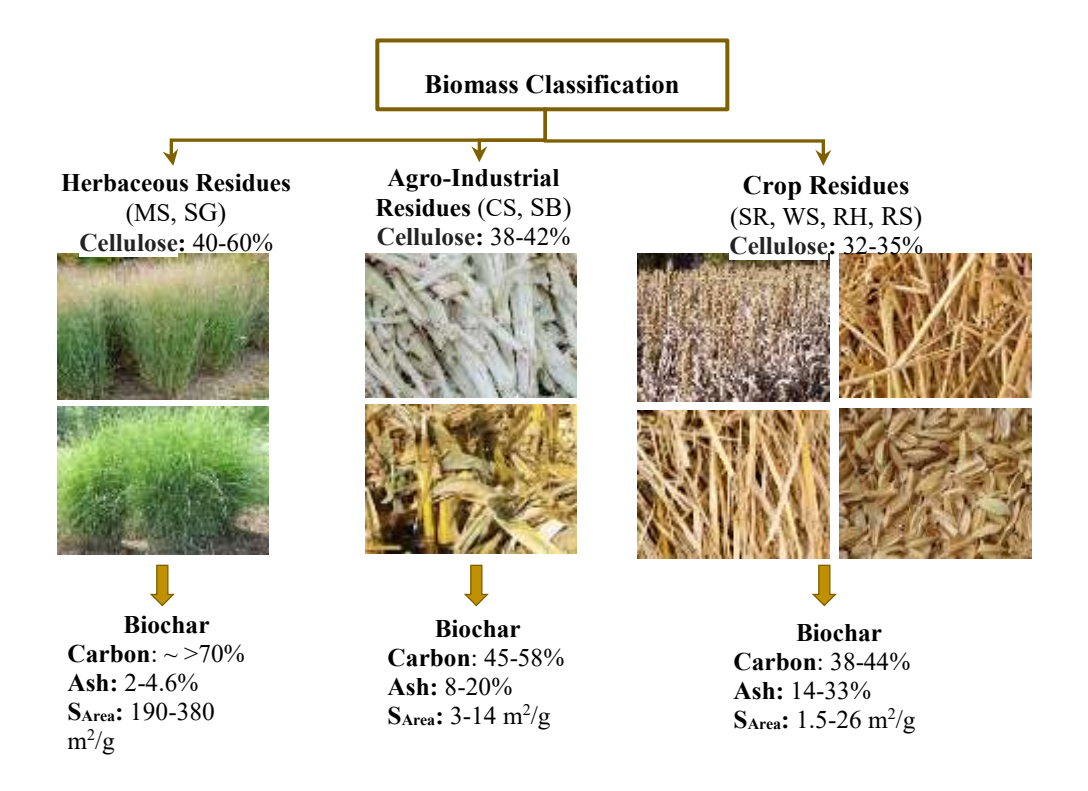


**Figure 1.** Schematic Representation of Biomass Classifications and the corresponding biochar Note: MS: Miscanthus; SG: Switch Grass; CS: Corn Stover; SB: Sugarcane Bagasse; SR: Sorghum; WS: Wheat Straw; RH: Rice Husk and RS: Rice straw.

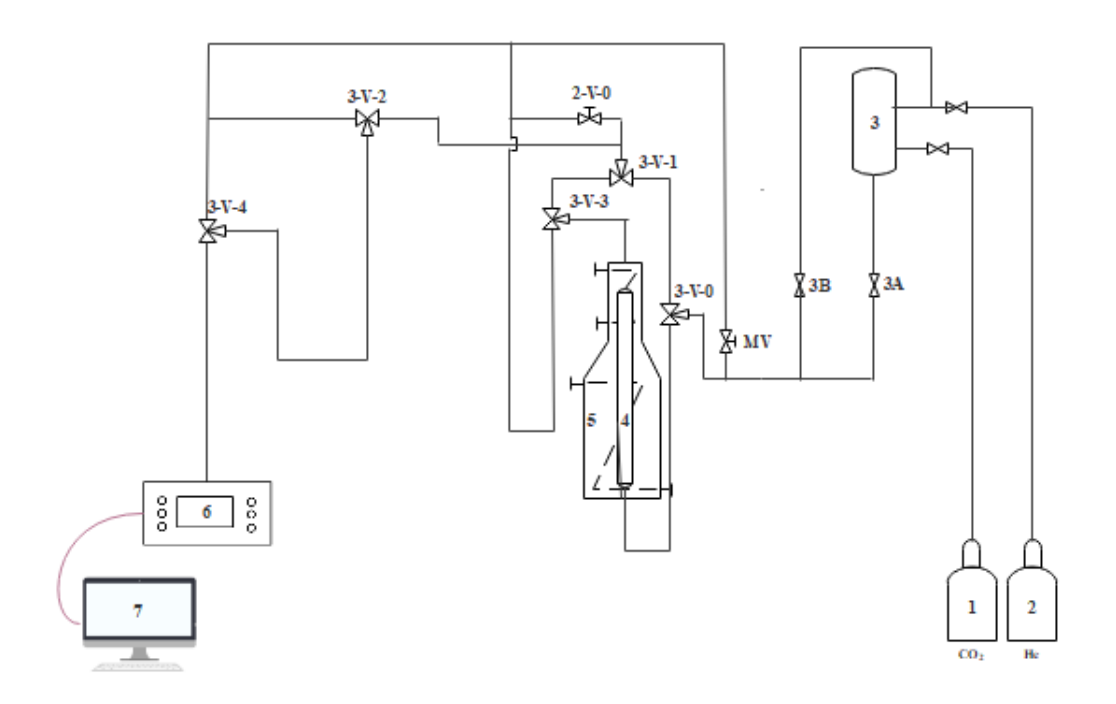


Figure 2. Schematic Representation of the Experimental Set-Up

1. CO<sub>2</sub> gas cylinder; 2. He gas cylinder; 3. Mixing Column; 4. Reactor Tube; 5. Furnace; 6. CO-CO<sub>2</sub> analyzer; 7. Computer; MV: Metering Valve

**Note:** Valve 3A: Allow the CO<sub>2</sub> gas flow to the column; Valve 3B: This valve allows helium gas flow to the column; Valve 2-V-0: Control outlet gas flow from column to analyzer; Valve 3-V-0: Switch the gas flow between column and analyzer; Valve 3-V-1: Switch flow of gas between inlet gas and outlet of the column during adsorption; Valve 3-V-2: Direct the sample gas towards analyzer; Valve 3-V-3: When turned towards the bypass it bypasses excess gas from the analyzer and when turned towards the analyzer it directs the sample gas towards the analyzer; Valve 3-V-4: Final tuning of the gas to the analyzer.

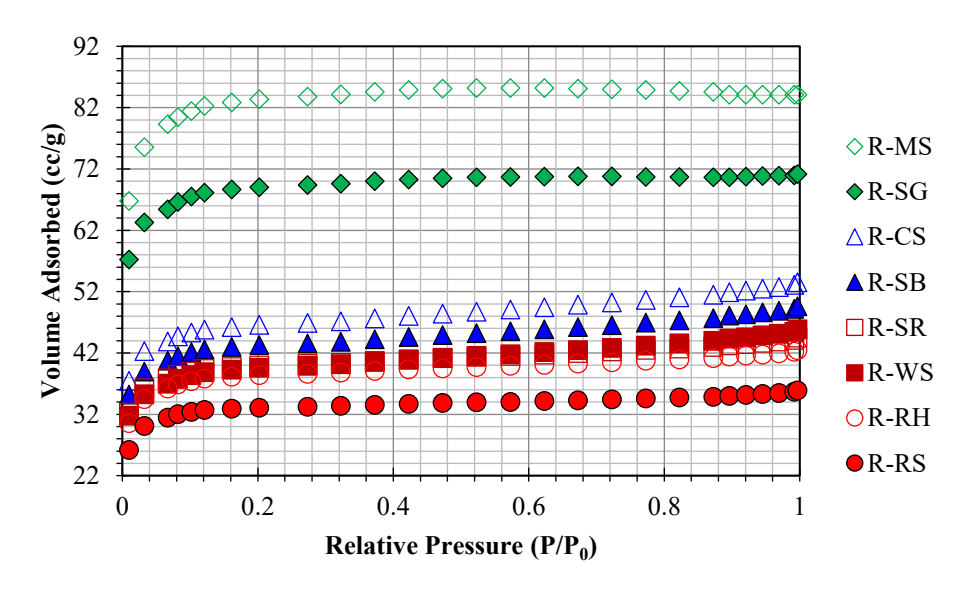
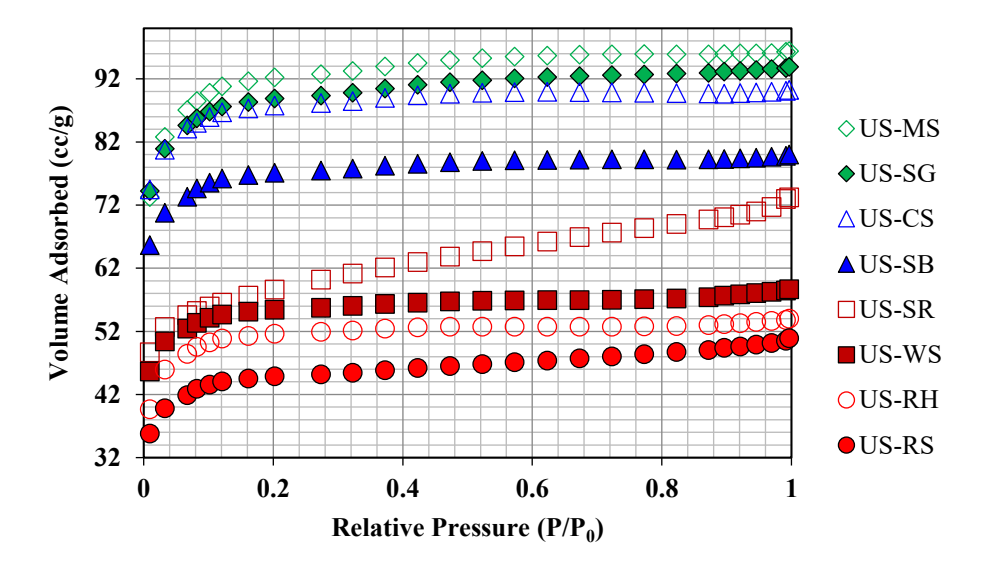
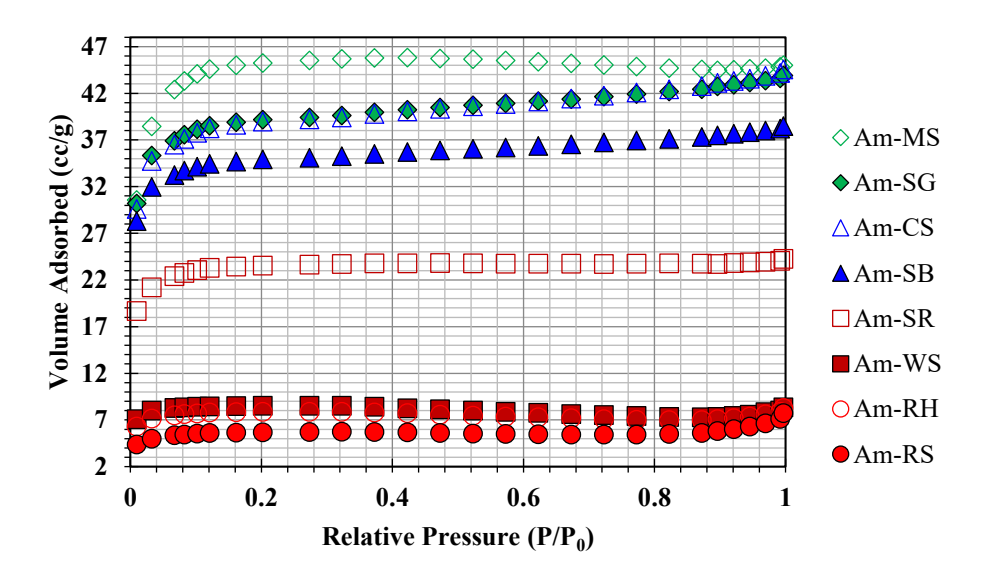


Figure 3. Adsorption isotherms of raw biochar samples



**Figure 4.** Adsorption isotherms for ultrasonic activated biochar samples but no amine. The adsorbed volume is higher than raw biochar samples indicating higher surface area.



**Figure 5.** Adsorption isotherms for amine activated biochar samples but no ultrasound. The adsorbed volume is lower than raw biochar samples because amine attached to the biochar surface and reduces surface area.

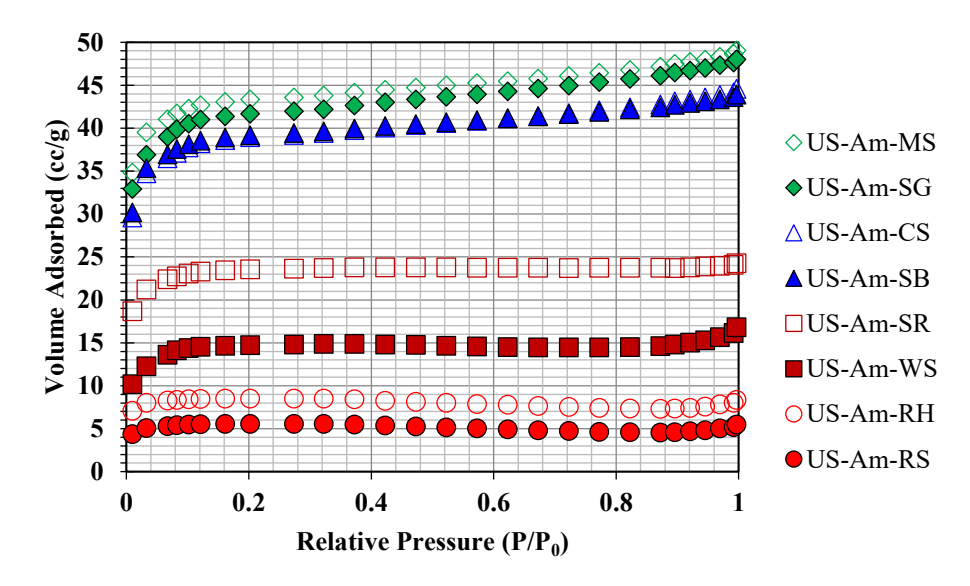
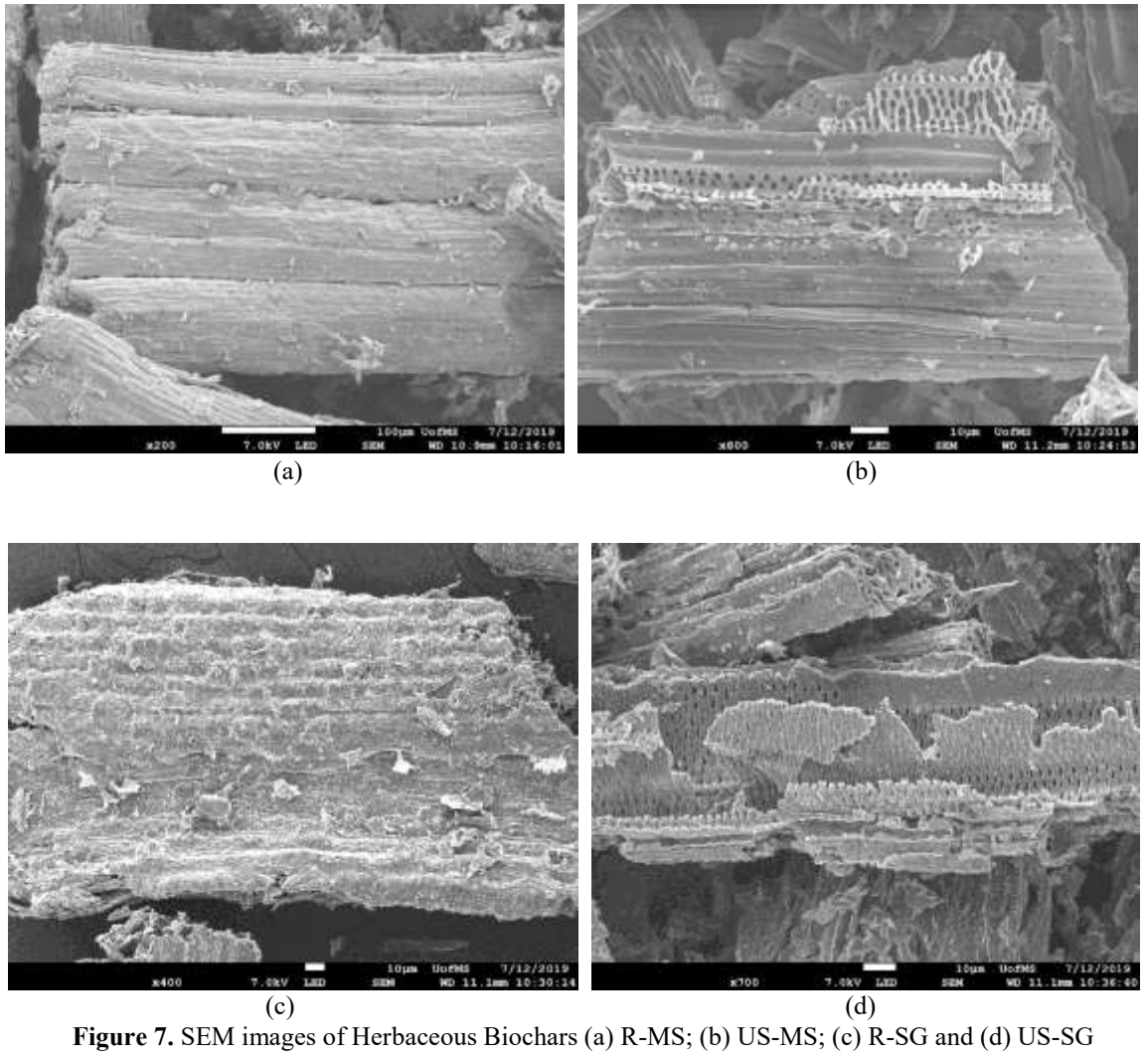


Figure 6. Adsorption isotherms of ultrasound-amine activated biochar samples. The adsorbed volume is lower than raw biochar samples but higher than aminated samples. Note: R: Raw: US: Ultrasound Activated; Am: Amine Activated



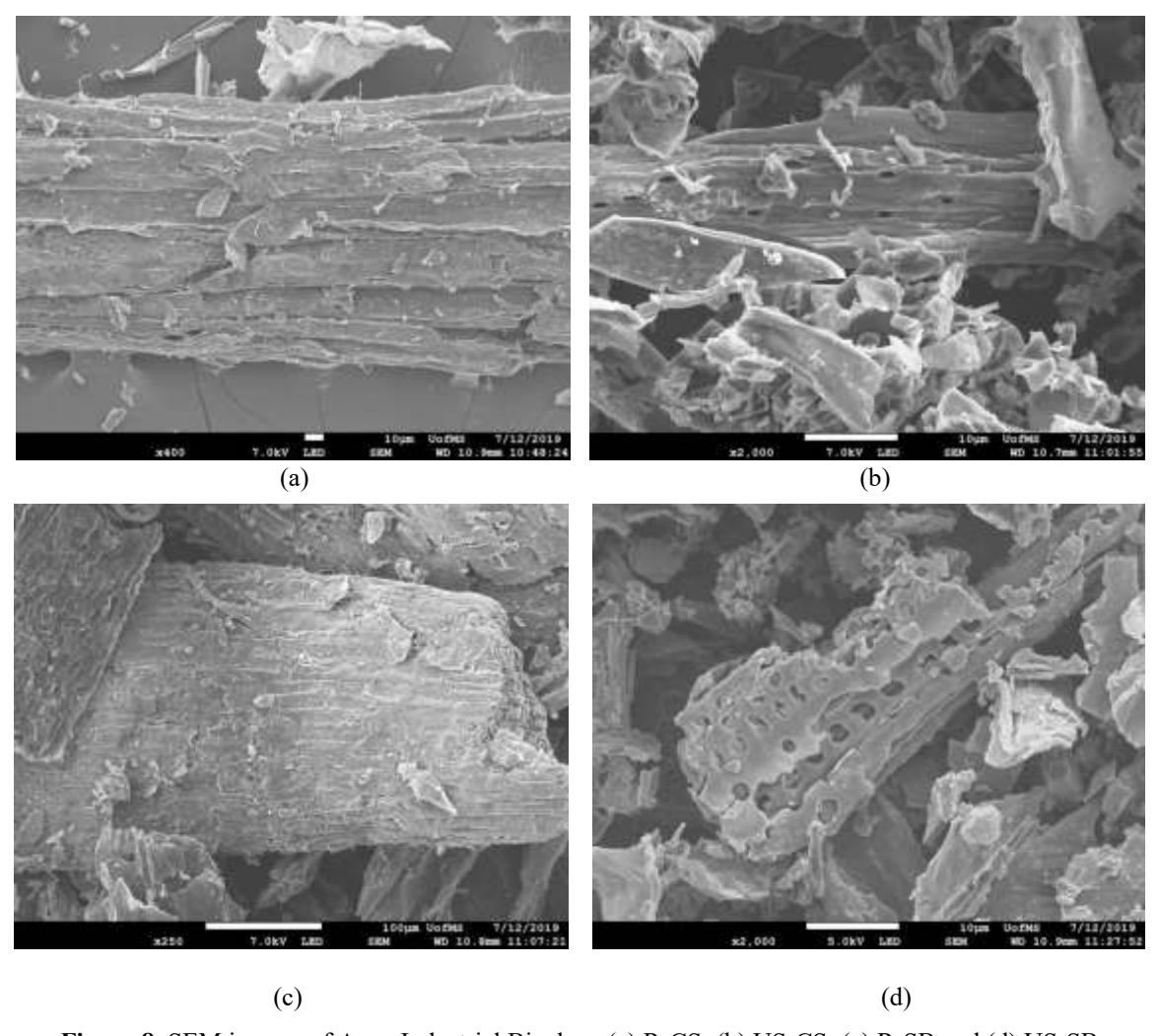
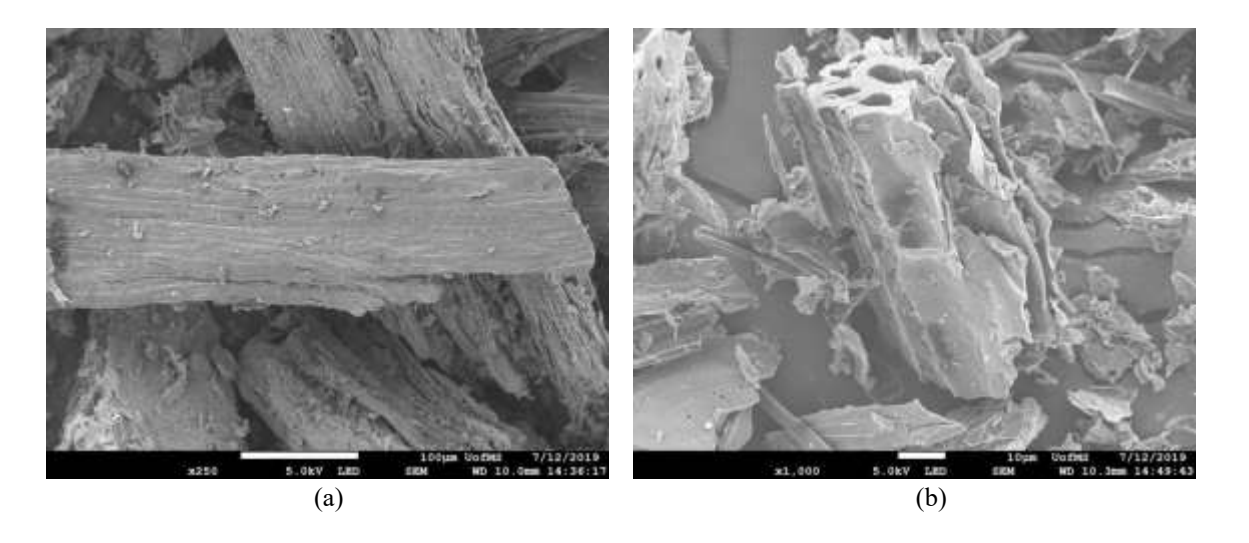
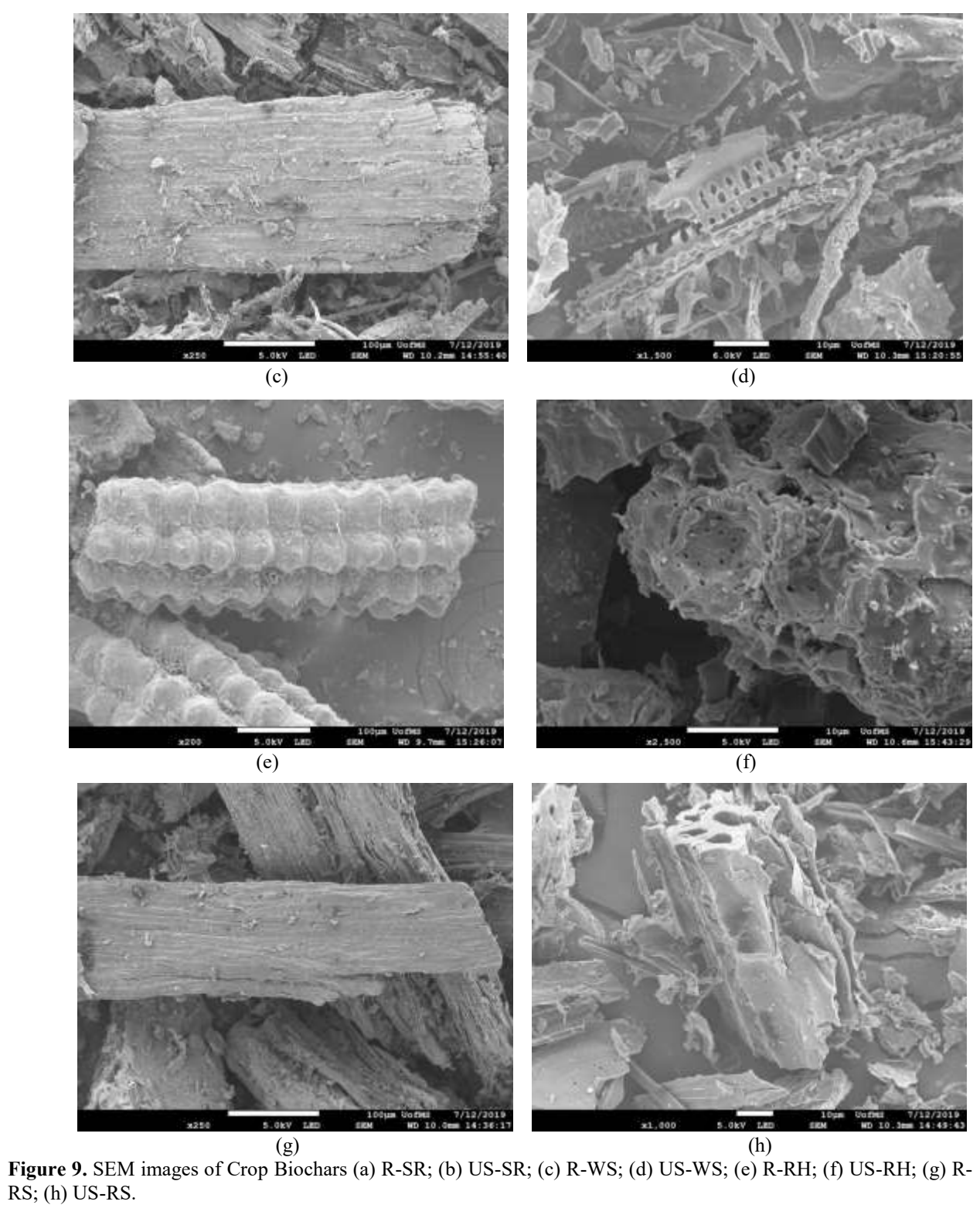
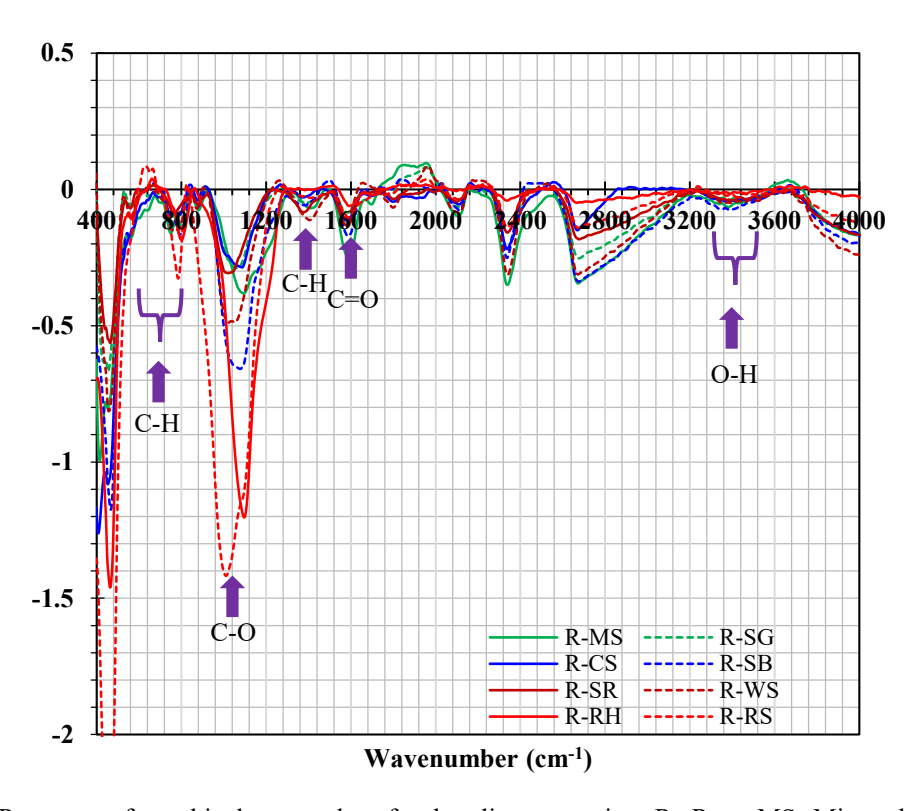


Figure 8. SEM images of Agro-Industrial Biochars (a) R-CS; (b) US-CS; (c) R-SB and (d) US-SB







**Figure 10.** FTIR spectra of raw biochar samples after baseline correction. R- Raw; MS: Miscanthus; SG: Switch Grass; CS: Corn Stover; SB: Sugarcane Bagasse; SR: Sorghum; WS: Wheat Straw; RH: Rice Husk and RS: Rice straw. Strong peaks at 1000-1100, 1600-1700, 2300 and 3300-3600 cm<sup>-1</sup> are ascribed to C-O, C=O, CO<sub>2</sub> and -OH stretching.

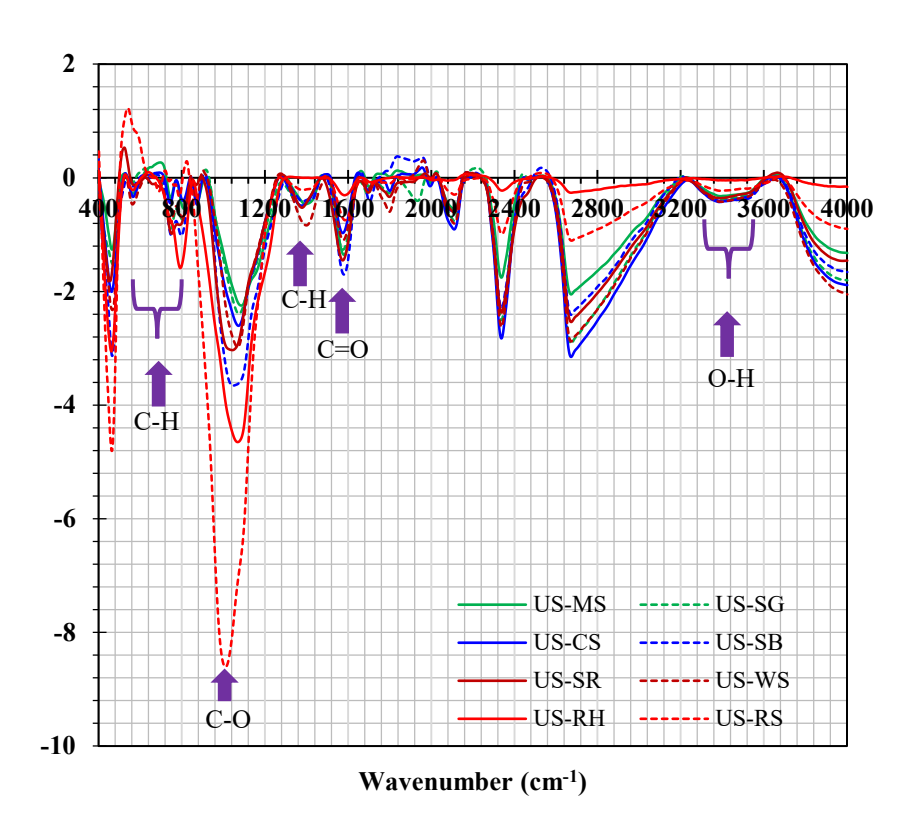


**Figure 11.** FTIR spectra of ultrasound activated biochar samples after baseline correction. US- Ultrasound. Physical activation made the peaks more intense and distinct specifically at 1100 (C-O), 1600 (C=O), and 3300-3600 cm<sup>-1</sup> (OH) that further demonstrate the importance of sonication in exfoliating biochar structure and making oxygen functionalities available.

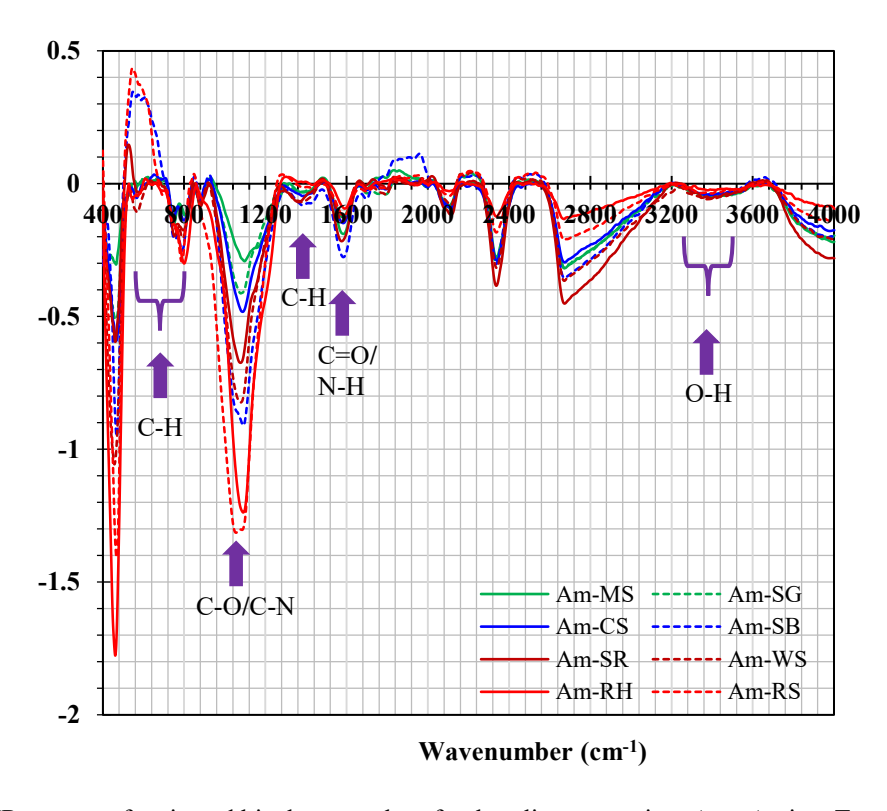


**Figure 12.** FTIR spectra of aminated biochar samples after baseline correction. Am- Amine. Two new peaks appear at 1000-1200 and 1600 cm<sup>-1</sup> for C-N and N-H and overlap with C-O and C=O peaks thus show intense peaks

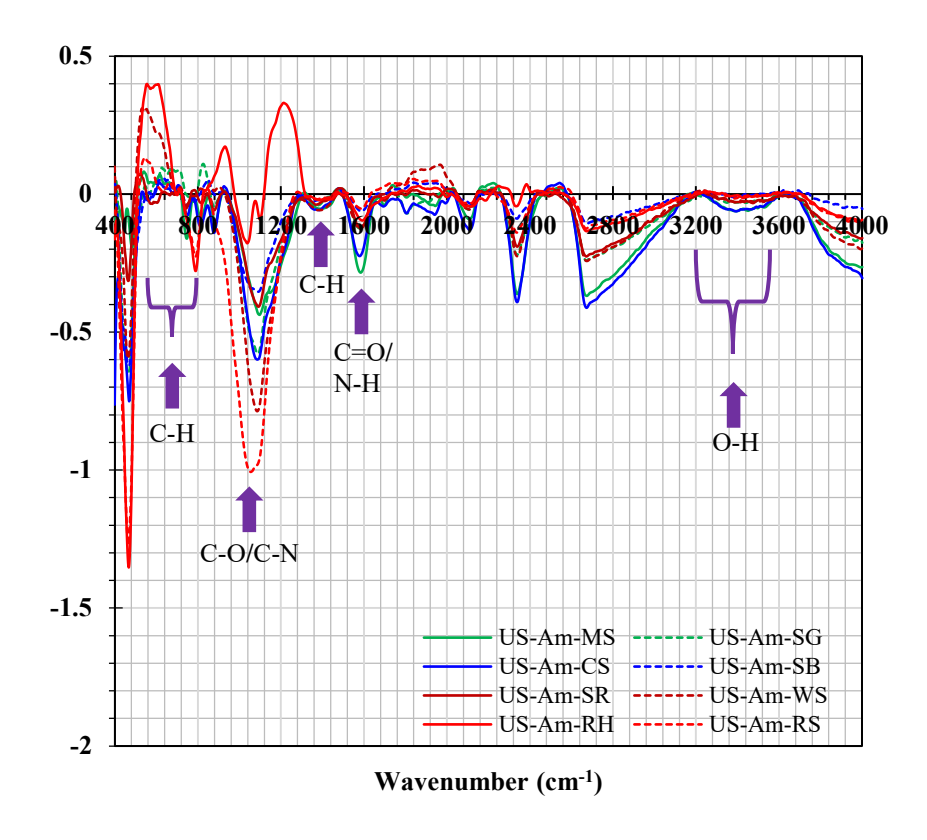


**Figure 13.** FTIR spectra of ultrasonicated-aminated biochar samples after baseline correction. US = ultrasound and Am = Amine. Two new peaks appear at 1000-1200 and 1600 cm<sup>-1</sup> for C-N and N-H similar to aminated samples.

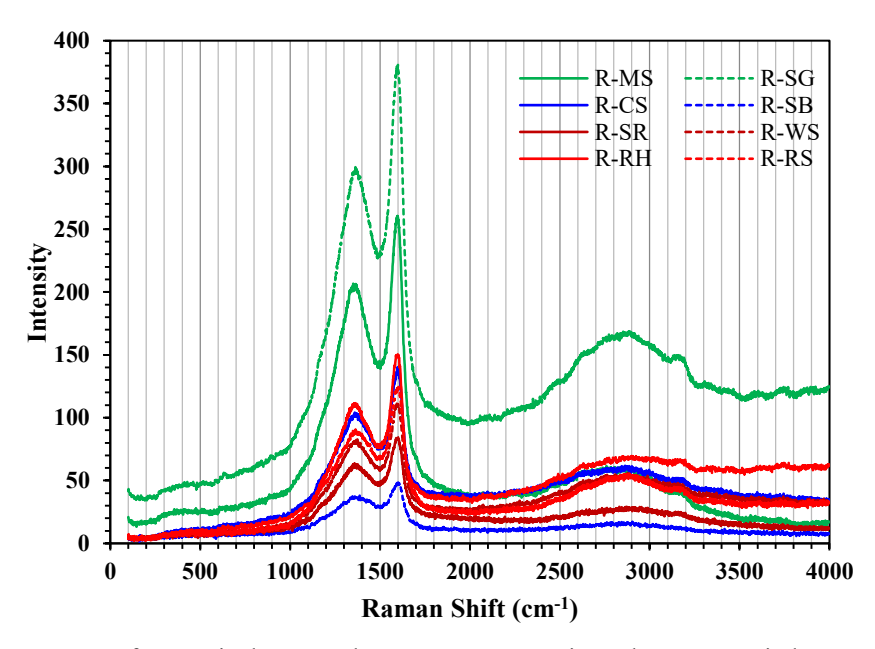


**Figure 14.** Raman Spectra of Raw Biochar Samples. R- Raw. MS: Miscanthus; SG: Switch Grass; CS: Corn Stover; SB: Sugarcane Bagasse; SR: Sorghum; WS: Wheat Straw; RH: Rice Husk and RS: Rice straw. Raw samples show very less intensities indicating their low intensity ratios as described in the results and discussion section

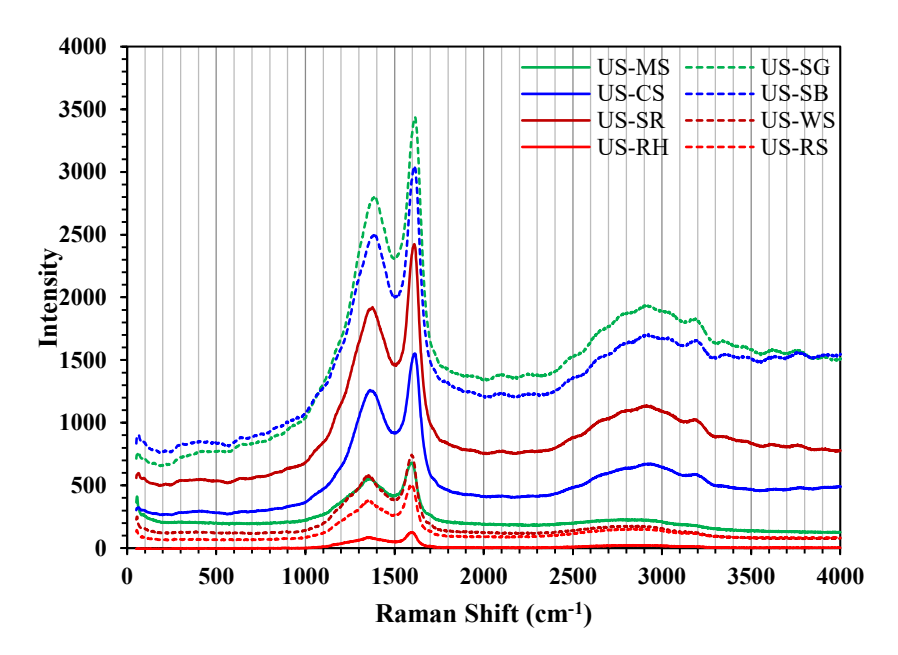


**Figure 15.** Raman Spectra of Physically Activated (no amine) Biochar Samples. US- Ultrasound. The treatment was done in the presence of ultrasound only. These tests were intended to determine the effect of physical activation alone on the graphitic structure of biochars. The treatments didn't show any significant change for intensity ratio measurement compared to chemically and sono-chemically modified biochars

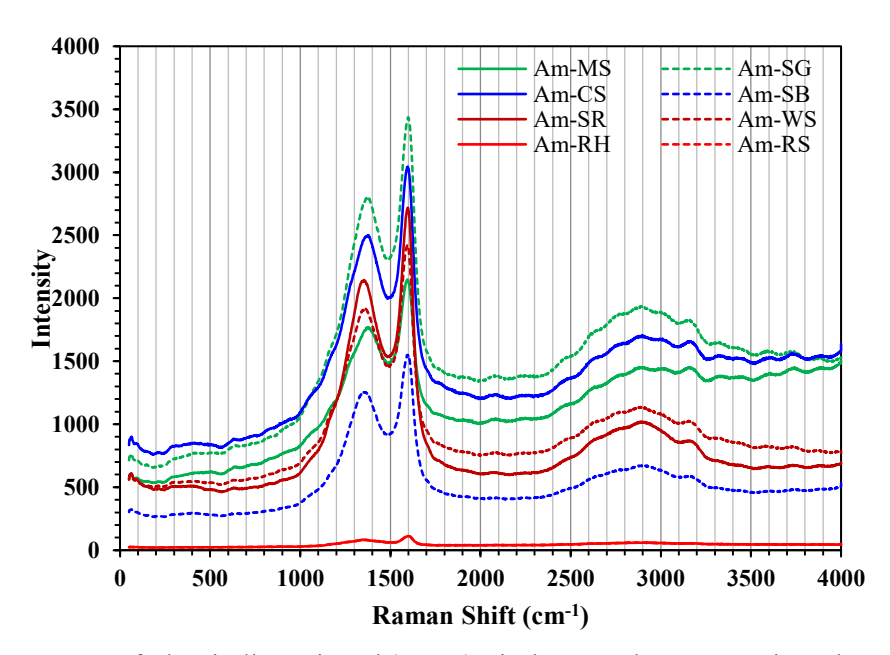


**Figure 16.** Raman Spectra of Chemically Activated (no US) Biochar Samples. Am- Amine. The treatment was done in the presence of amine only. These tests were intended to determine the effect of amine functionalization alone on the graphitic structure of biochars. The treatments show comparable differences specifically for herbaceous (MS, SG) and agro-industrial (CS, SB) based biochars

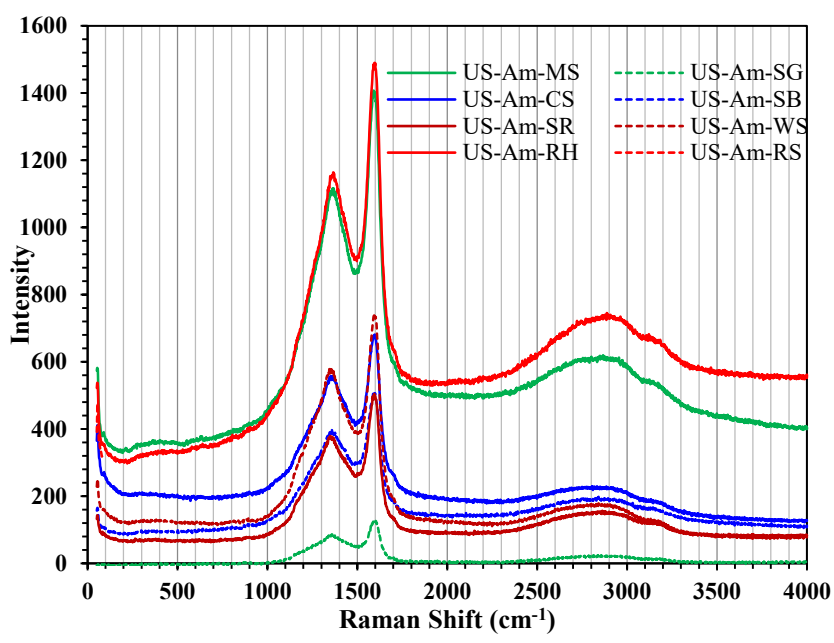


**Figure 17.** Raman Spectra of Sono-Chemically Activated Biochar Samples. US- Ultrasound and Am- Amine. The activation was done physico-chemically i.e. first physical activation in presence of acoustic field followed by chemical functionalization using amine. The treatments resulted to the changes in intensity ratio with the highest possible intensity ratio for miscanthus and lowest possible for rice straw

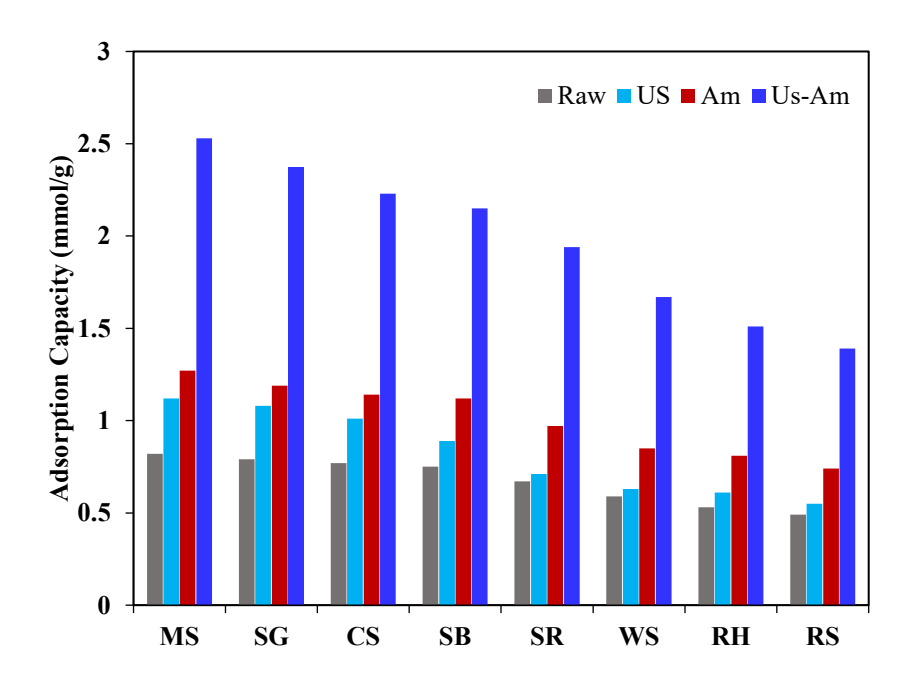


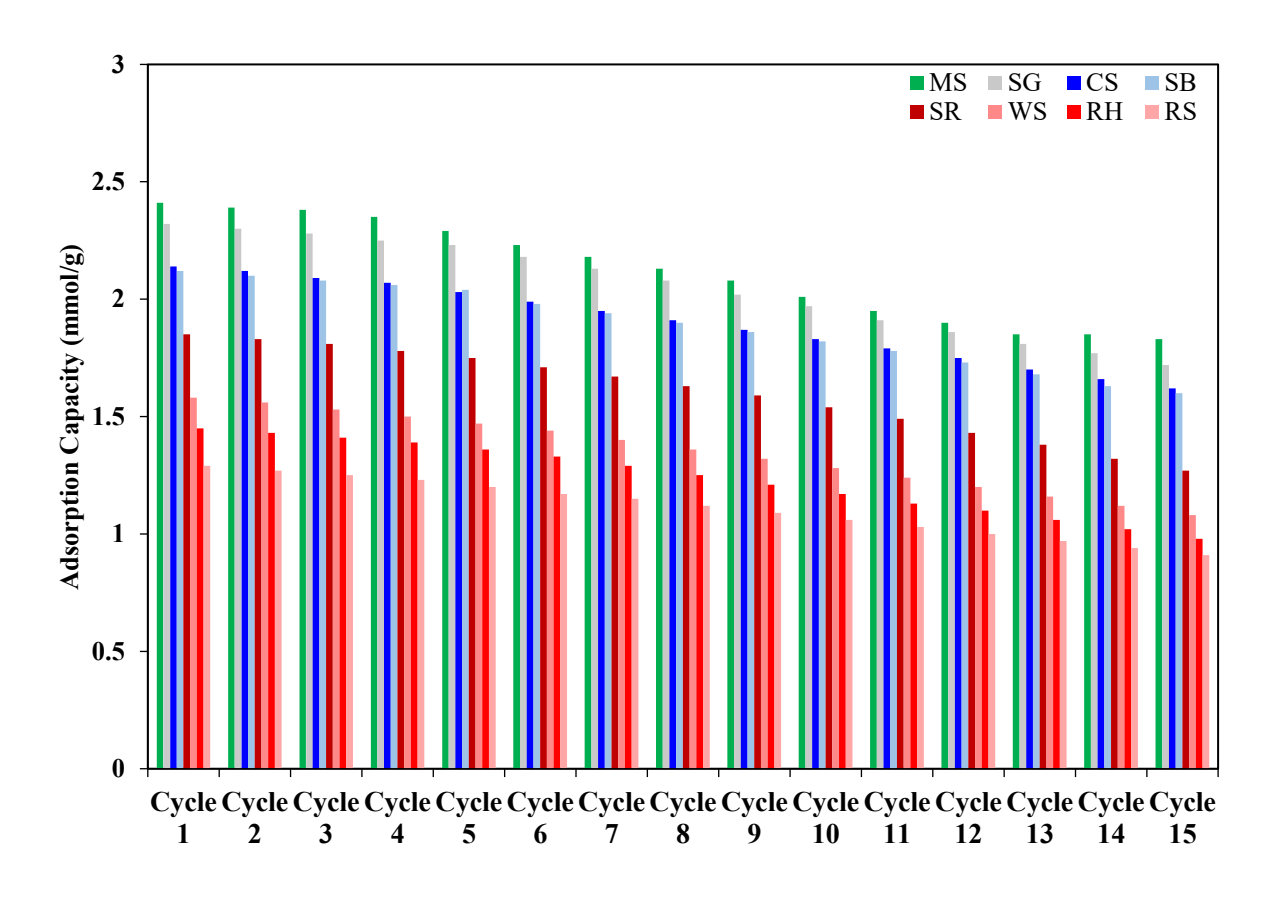
Figure 18. Adsorption capacities of different biochars at 70 °C and 10 vol% CO₂ inlet concentration. ■ Raw biochars, ■ Acoustic activated biochar ■ chemically activated biochar, ■ sono-chemically activated biochar. herbaceous residues (MS:miscanthus and SG: switchgrass), agro-industrial residues (CS: corn stover, SB: sugarcane bagasse and), crop residues (SR: sorghum, WS: wheat straw, RH: rice husk, RS: rice straw).

Figure 19. Postulated Mechanism of Char Formation under Different Activation Conditions

Scheme 1: For Terminal Amino Group

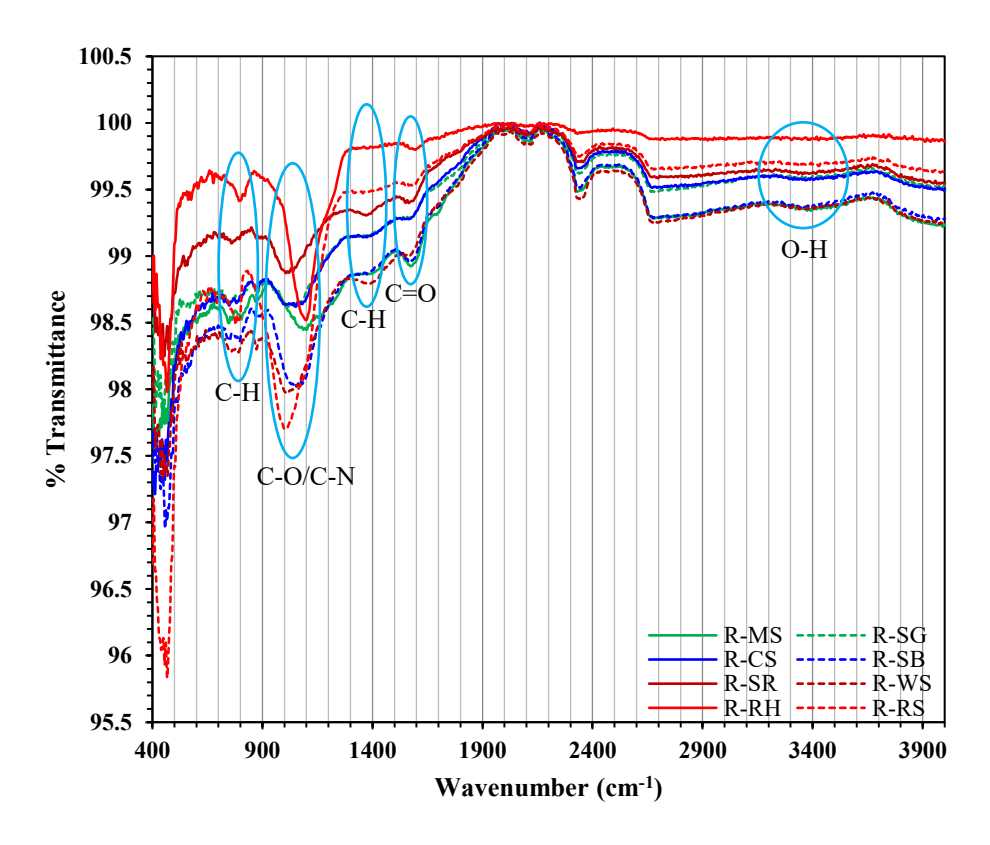
Scheme 2: For Intermediate Amino Group

Figure 20. Mechanism of Zwitterion and Alkyl Carbamate formation during the Interaction between Biochar Chemical Structure (C and N) with CO<sub>2</sub>



**Figure 21:** Cyclic adsorption-desorption behavior of ultrasono-aminated Herbaceous residue based chars (MS, SG), Agro-industrial based biochars (CS and SB) and Crop residue based biochars (SR, WS, RH and RS)

## **Supplementary Documents**



**Figure 22.** FTIR Spectra of Raw Biochar Samples. R- Raw; MS: Miscanthus; SG: Switch Grass; CS: Corn Stover; SB: Sugarcane Bagasse; SR: Sorghum; WS: Wheat Straw; RH: Rice Husk and RS: Rice straw. The transmittance of all raw biochar samples is reported in 400-4000 cm<sup>-1</sup> range. Strong peaks at 1100, 1600 cm<sup>-1</sup> and 3300-3600 cm<sup>-1</sup> are ascribed to C-O, C=O and -OH stretching

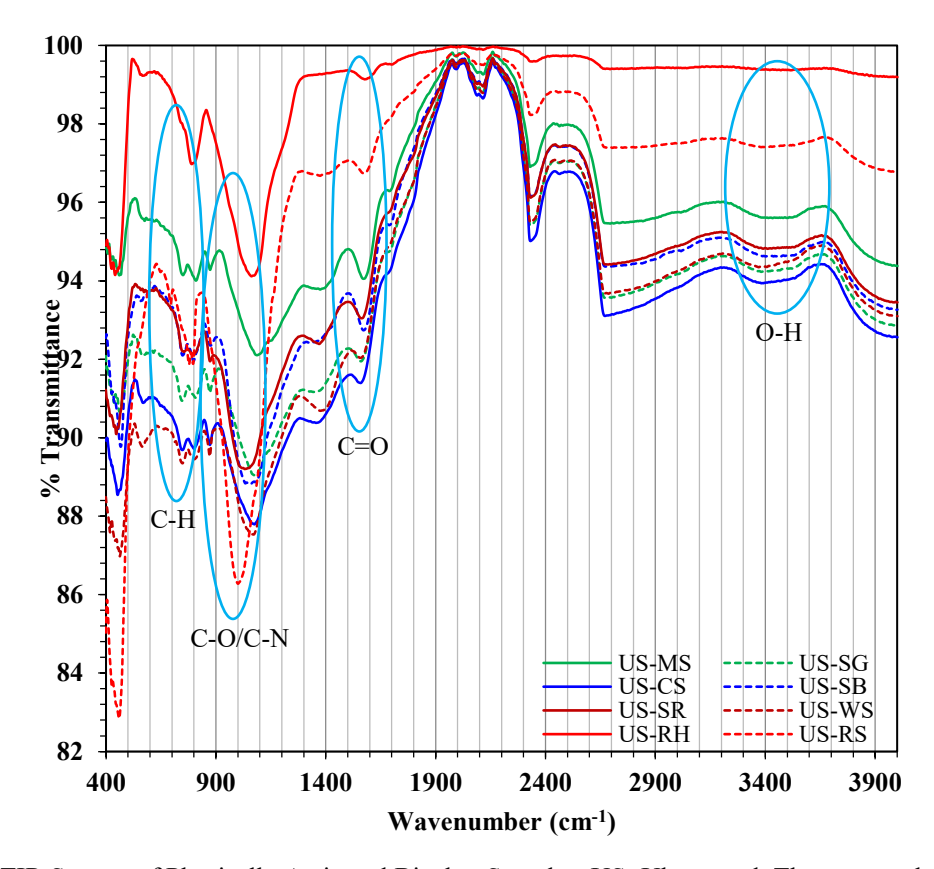
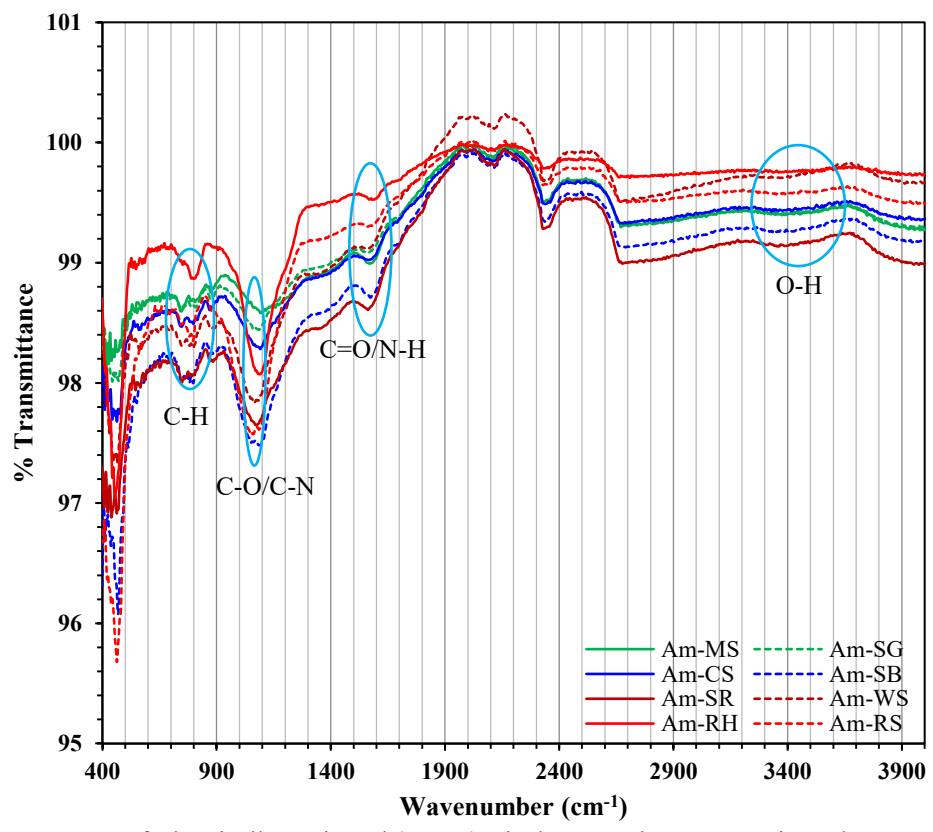
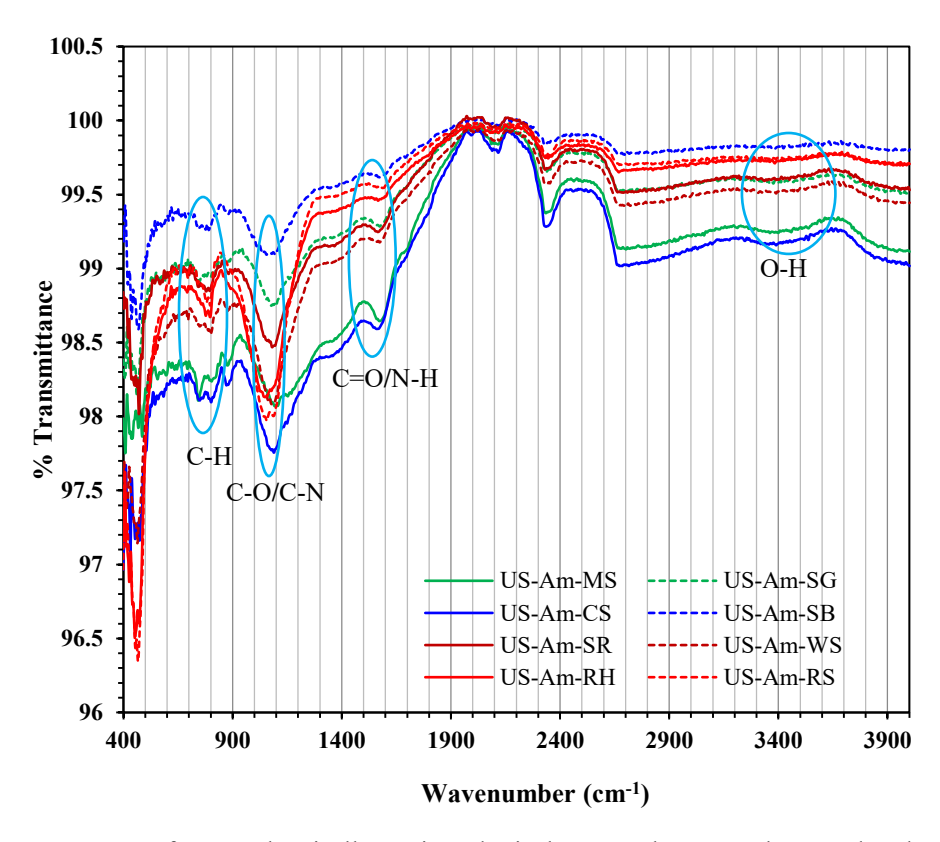


Figure 23. FTIR Spectra of Physically Activated Biochar Samples. US- Ultrasound. The spectra show similar peaks as observed for raw biochars samples. However, acoustic treatment made the peaks more intense and distinct. For instance, peaks at  $\sim 800$  and  $1000~\rm cm^{-1}$  (attributed as aromatic C-H deformation and -COOH group) became stronger and visible upon sonication. Similar behavior has been observed for peak at  $3300-3600~\rm cm^{-1}$  (-OH stretching) that further demonstrate the importance of sonication, exfoliating biochar structure and making oxygen functionalities available



**Figure 24.** FTIR Spectra of Chemically Activated (no US) Biochar Samples. Am- Amine. The treatments were done in the presence of amine only. These tests were intended to determine the effect of amine alone on the surface functionalities of biochars. The treatments resulted to the changes in the IR peaks primarily for hydroxyl group in region of 3300-3600 cm<sup>-1</sup>, carbonyl at 1605 cm<sup>-1</sup> and formation of new bonds at 1000-1200 and 1500-1600 cm<sup>-1</sup>. Although these changes are not clearly visible in this figure but are observable in Fig 3 after baseline correction.



**Figure 25.** FTIR Spectra of Sono-Chemically Activated Biochar Samples. US- ultrasound and Am- Amine. The activation was done physico-chemically i.e. first physical activation in presence of acoustic field followed by chemical functionalization using amine. The peaks do not have significant changes compared to the aminated samples. The only observed difference is the formation of new bonds for C-N and N-H.

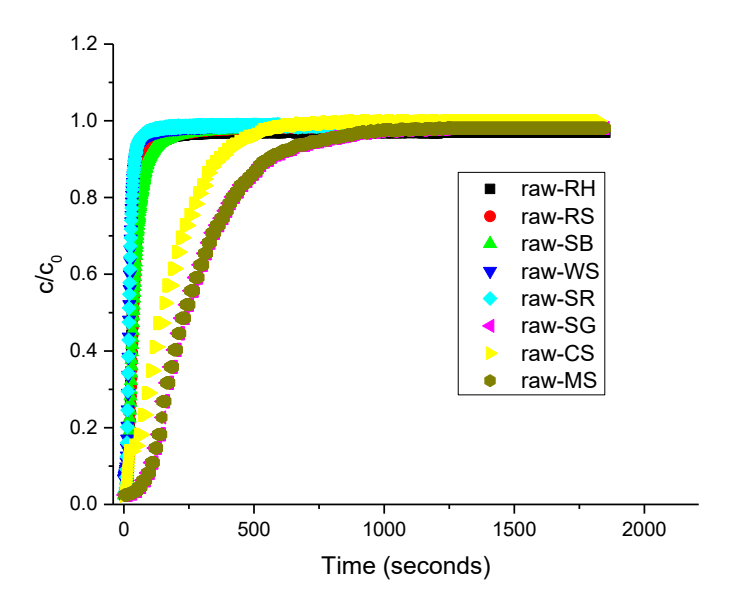


**Figure 26.** Adsorption Breakthrough Curves for Raw Biochar Samples. CS: Corn Stover; RH: Rice Husk; SB: Sugarcane Bagasse; SR: Sorghum; MS:Miscanthus; RS: Rice straw; SG: Switch Grass and WS: Wheat Straw

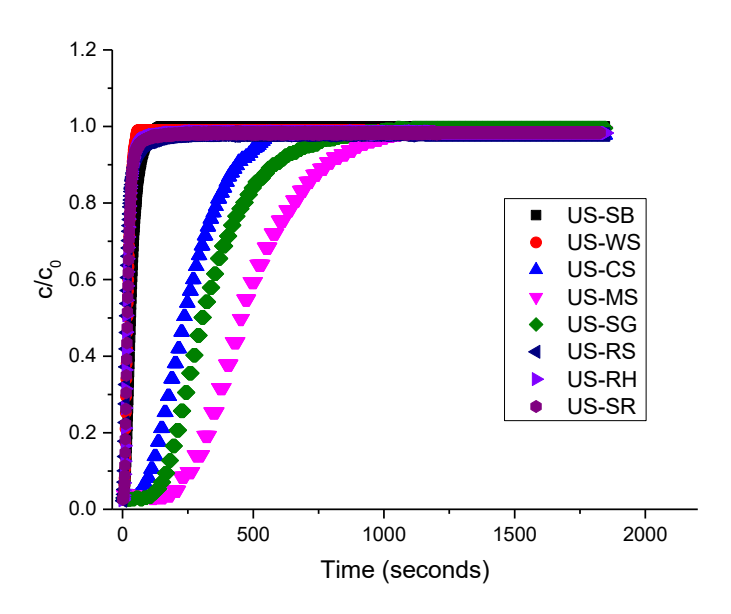


**Figure 27.** Adsorption Breakthrough Curves for Physically Activated (Ultrasound Treated) Biochar Samples. CS: Corn Stover; RH: Rice Husk; SB: Sugarcane Bagasse; SR: Sorghum; MS: Miscanthus; RS: Rice straw; SG: Switch Grass and WS: Wheat Straw

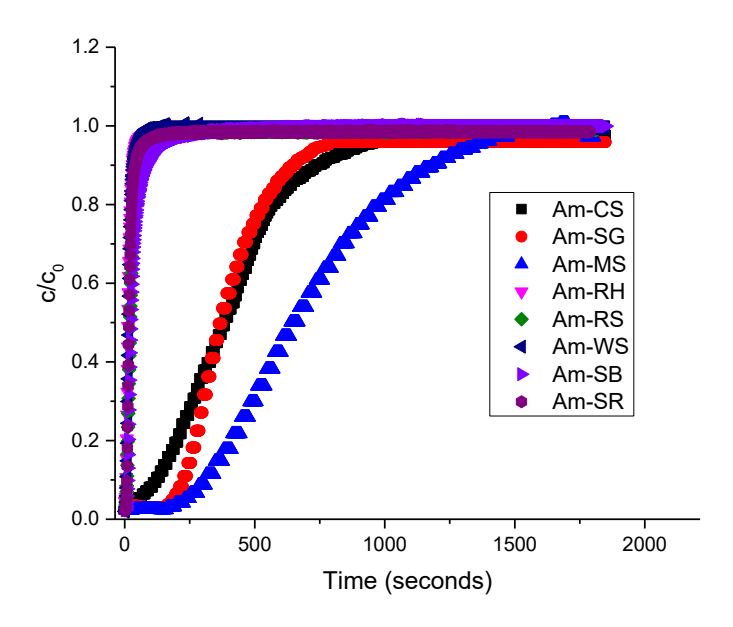


**Figure 28.** Adsorption Breakthrough Curves for Chemically Activated (Amine Only) Biochar Samples. CS: Corn Stover; RH: Rice Husk; SB: Sugarcane Bagasse; SR: Sorghum; MS:Miscanthus; RS: Rice straw; SG: Switch Grass and WS: Wheat Straw

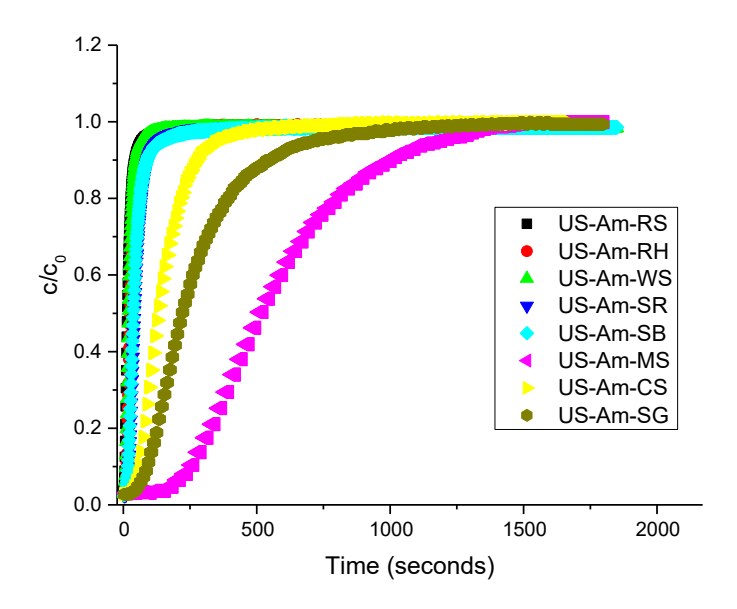


**Figure 29.** Adsorption Breakthrough Curves for Sono-Chemically Activated (Ultrasound and Amine) Biochar Samples. CS: Corn Stover; RH: Rice Husk; SB: Sugarcane Bagasse; SR: Sorghum; MS:Miscanthus; RS: Rice straw; SG: Switch Grass and WS: Wheat Straw